Volume 14
Number 11
21 March 2022
Pages 3975-4350

Nanoscale

rsc.li/nanoscale

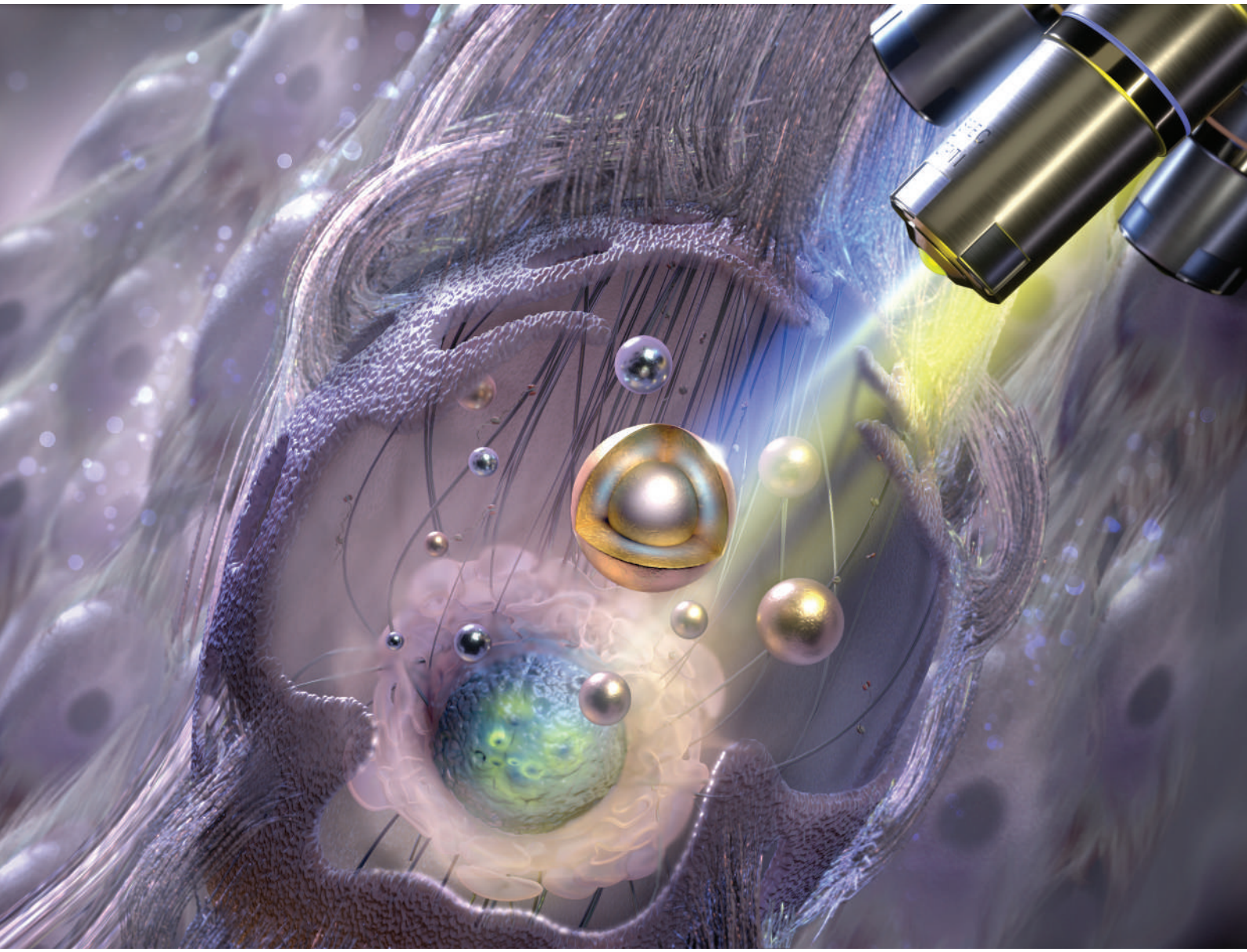

ISSN 2040-3372

ROYAL SOCIETY OF CHEMISTRY

COMMUNICATION
Surya M. Nauli *et al.*
The use of advanced spectral imaging to reveal nanoparticle identity in biological samples

NCNST

Nanoscale

ROYAL SOCIETY OF CHEMISTRY

COMMUNICATION

Cite this: *Nanoscale*, 2022, **14**, 4065

Received 15th November 2021,
Accepted 24th January 2022

DOI: 10.1039/d1nr07551a

rsc.li/nanoscale

The use of advanced spectral imaging to reveal nanoparticle identity in biological samples†

Qamar A. Alshammari,‡[a,b] Rajasekharreddy Pala,‡[a] Ayan K. Barui,[a] Saud O. Alshammari,[a,c] Andromeda M. Nauli,[d] Nir Katzir,[e] Ashraf M. Mohieldin[a] and Surya M. Nauli *[a,f]

Nanoparticles (NPs) have been used in drug delivery therapies, medical diagnostic strategies, and as current Covid-19 vaccine carriers. Many microscope-based imaging systems have been introduced to facilitate detection and visualization of NPs. Unfortunately, none can differentiate the core and the shell of NPs. Spectral imaging has been used to distinguish a drug molecule and its metabolite. We have recently integrated this technology to a resolution of 9 nm by using artificial intelligence-driven analyses. Such a resolution allowed us to collect many robust datapoints for each pixel of an image. Our analyses could recognize 45 spectral points within a pixel to detect unlabeled Ag-NPs and Au-NPs in single live cells and tissues (liver, heart, spleen and kidneys). The improved resolution and software provided a more specific fingerprinting for each single molecule, allowing simultaneous analyses of 990 complex interactions from the 45 points for each molecule within a pixel of an image. This in turn allowed us to detect surface-functionalization of Ag-NPs to distinguish the core from the shell of Ag-NPs for the first time. Our studies were validated using various laborious and time-consuming conventional techniques. We propose that spectral imaging has tremendous potential to study NP localization and identification in biological samples at a high temporal and spatial resolution, based primarily on spectral identity information.

[a]*Department of Biomedical & Pharmaceutical Sciences, Harry and Diane Rinker Health Science Campus, Chapman University, 9401 Jeronimo Road, Irvine, CA 92618-1908, USA. E-mail: nauli@chapman.edu, snauli@uci.edu; Fax: +1 714-516-5481; Tel: +1 714 -516-5480*

[b]*Department of Pharmacology and Toxicology, Faculty of Pharmacy, Northern Border University, Kingdom of Saudi Arabia*

[c]*Department of Plant Chemistry and Natural Products, Faculty of Pharmacy, Northern Border University, Kingdom of Saudi Arabia*

[d]*Department of Biomedical Sciences, Western Michigan University, Homer Stryker M.D. School of Medicine, Kalamazoo, MI 49008, USA*

[e]*Applied Spectral Imaging, 5315 Avenida Encinas, Suite 150, Carlsbad, CA 92008, USA*

[f]*Department of Medicine, University of California Irvine, Irvine, CA 92868, USA*

†Electronic supplementary information (ESI) available. See DOI: 10.1039/d1nr07551a

‡Authors contributed equally to this work.

Introduction

Conventional methods used for the quantification of inorganic NPs include inductively-coupled plasma mass spectrometry (ICP-MS) and inductively-coupled plasma atomic emission spectroscopy (ICP-AES).[1–3] In addition to the matrix interference, some disadvantages in ICP-associated methods include chemical interference, the necessity of liquidized samples, low plasma sensitivity to organic solvents, and ineffectiveness of the nebulizer. To overcome these drawbacks, non-destructive techniques have also been developed. These include the use of fluorescent-labeled NPs[4,5] and the modern ultrasonic holography.[6,7]

While fluorescent-conjugated NPs are generally used to identify NP localization in live biological samples, such conjugation could interfere with NP function, localization, cytotoxicity and biodistribution.[8–10] Thus, different imaging modalities have been recently introduced to image unlabeled-NPs without destroying biological tissues. Based on the light-refractive index of NPs, NP detection in live cells has been performed.[11] The specific scattered-light of NPs allows real-time monitoring of unlabeled NPs.[12] In addition to Raman spectroscopy,[13] standard optical spectroscopic microscopy has also been used to image NPs, albeit this was done at a much narrower scanning range of 200 nm.[14] Different optical microscopy techniques, used to detect a specific spectrum for NPs, have therefore been proposed to capture absorption spectra[15] and the plasmon resonance scattering or extinction spectra of various NPs.[16–19]

Despite recent advances in optical microscopes, visualizing unlabeled-NPs remains a challenge. This is primarily due to intensity-based measurements performed at a very narrow spectrum optimized for different studies and systems at different laboratories. We recently introduced a spectral imaging system in which broader spectral characteristics are first identified, characterized and stored in a library.[20] Unlike other previous studies, however, our current studies did not identify a molecule based merely on the spectral intensity,

relative intensity, or spectral points. Our new strategies using a higher spectral resolution and artificial intelligence for point recognition improved our capability to differentiate two very similar molecules.

Results

We can now scan absorbance spectra from 400 nm to 800 nm with a resolution of 9 nm (ESI Fig. 1†). This improved spectral imaging provides much more detailed information for a more accurate image analysis, resulting in 45 unique spectral points for each pixel. These points are interconnected resulting in 990 unique interactions (ESI Fig. 2†). Using artificial intelligence-driven analysis to recognize relative interactions between 2 points, the integrations of such interactions provide unique fingerprints for different chemicals. The key feature is that we could recall all these specific interactions from the library fairly quickly. These relative interaction points become the unique identity (or fingerprint) of a molecule.

We report here that spectral imaging can provide a high temporal and spatial resolution of silver nanoparticles with a shell (Ag(s)-NPs) or without a shell (Ag-NPs). Our validation results on gold nanoparticles (Au-NPs) are located mainly in the supplementary information. These NPs were characterized for their syntheses, hydrodynamic sizes and structural compositions (ESI Fig. 3;† see Method).

Spectral signatures of Ag(s)-NPs and Ag-NPs were identified with a major peak at 420 nm

Using a microscope equipped with hyperspectral imaging (GenASIs from Applied Spectral Imaging), we imaged and recorded the spectral characteristics of the clusters of Ag(s)-NPs before and after incubation with cells (Fig. 1a). We captured the spectral range between 400 and 800 nm for Ag(s) NPs in the presence and absence of cells. Ag(s)-NPs had characteristic spectra with a distinctive peak at 420 nm (Fig. 1b). This peak was consistent with a previous study.[21] While this peak was the main characteristic of Ag(s)-NPs, we also looked at different features that could contribute to the characteristics of Ag(s)-NPs. Interestingly, we could generate two distinct libraries for Ag(s)-NPs. The peak of Ag(s)-NPs could be distinctively differentiated by an additional "shoulder" that only appeared at the peripheral or shell of the NPs. Of note, silver–polymer core–shell NPs are generally known for their unique optical properties, in which the shell of Ag also plays a critical role in protecting the Ag core.[22,23] A shift in the shoulder peak could therefore be used to differentiate the core and shell of Ag-NP clusters. We quantified the spectral intensities of these peaks before and after 18-hour incubation with cells (Fig. 1c). As verified by traditional spectrophotometry, the linearity of Ag(s)-NPs was observed with a peak at 420 nm (ESI Fig. 4a†), indicating that we could predict the singularity or number of NPs in each pixel of an image based on the peak intensity of the spectra. Extrapolating from these intensity differences, our data suggested that Ag(s)-NPs tended to aggregate more in solution than in cells (Fig. 1d).

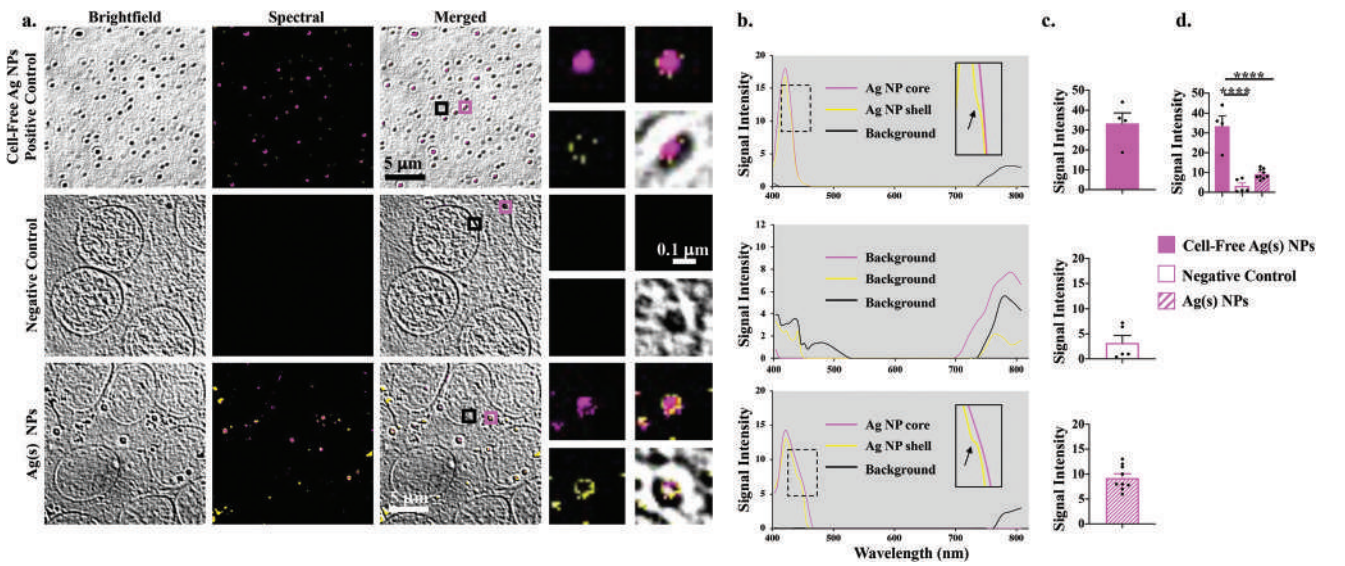

Fig. 1 Identification of the spectra of Ag(s)-NPs. (a) Brightfield images of the Ag(s)-NPs in the cell-free system (positive control), fixed cells (negative control), and 16-hour Ag(s)-NPs-treated cells (Ag(s)-NPs). The spectral images were extracted from the spectra library for the Ag(s)-NPs. Merged images illustrate superimposed brightfield and spectral images. The pink spectral image exhibits the core area of the Ag(s)-NP cluster, while the yellow color represents the shell region. (b) The graphs illustrate the wavelength peaks at ~420 nm for the positive control and the incubated cells. The pink wavelength displays the intensity of the core area and the yellow wavelength shows the shell part (with a small shoulder; insert and arrow). The black color exhibits the spectrum of the background area. The negative control spectra were identified based on unmatched spectra from our libraries. (c) The bar graphs show the variation of intensity data points at 420 nm. (d) The signal intensities were compared among cell-free positive control, non-treated cells negative control, and Ag(s)-NPs-treated cells. N = 4–5 for each positive and negative controls; N = 8 for experimental groups. ****, $P < 0.0001$.

To confirm our observation of Ag(s)-NPs, we synthesized Ag-NPs exclusively without the shell. The spectral characteristics of the Ag-NPs before and after incubation with cells were recorded (ESI Fig. 5a†). The Ag-NPs have the same characteristic spectra of Ag(s)-NPs, at ~420 nm, except that Ag-NP spectra were revealed without the additional "shoulder" (ESI Fig. 5b†). We also calculated the spectral intensities of these peaks before and after 18-hour incubation with cells (ESI Fig. 5c†). This revealed the specificity of spectral imaging to differentiate between the spectral characteristics of different types of silver NPs (Ag-NPs and Ag(s)-NPs).

Spectral signature of Au-NPs was identified with a major peak at 552 nm

Another inorganic NP was prepared to further confirm the capabilities of spectral imaging to identify a different NP, Au-NPs (ESI Fig. 6a†). Capturing spectra between 400 and 800 nm revealed that the Au-NPs had a unique spectral peak located between 520 and 580 nm (ESI Fig. 6b†), consistent with a previous study.[24] Background spectra without or with cells were captured to differentiate the spectral intensity of a peak at 552 nm (ESI Fig. 6c†). The specific subcellular localization of Au-NPs in the cells could be determined by examining the spectral characteristics of each pixel in the image. In the fixed cells, after treatment with Au-NPs for 18 hours, we could detect individuals or clusters of Au-NPs. To independently verify the microscopy spectra, we examined the spectra of Au-NPs using traditional spectrophotometry (ESI Fig. 4b†). The linearity of Au-NPs was observed with a peak at 536 nm, indicating that we could predict the singularity or number of NPs in each pixel of an image based on the peak intensity of the spectra. Extrapolating from these data, our studies suggested that Au-NPs tended to disperse more readily in cells than in solution (ESI Fig. 6d†).

Spectral imaging showed dynamic Ag(s)-NP or Au-NP accumulation in the cell nucleus

Once the spectral signatures for both Ag(s)-NPs and Au-NPs were identified and defined in the libraries, analytical software was used to perform spectral identity for each pixel of an image in order to identify pixels with the spectral resemblance of Ag(s)-NPs or Au-NPs. Background spectral characteristics could be taken from the non-treated cells (negative control) or different areas within the field of view in the image (see Method). This was a powerful method to trace non-fluorescence inorganic substances. We thus applied this technique to the time-lapse imaging of cells treated with 0.1 mg Ag(s)-NPs in 2 mL cell media (Fig. 2a; ESI Fig. 7†). We observed the continuous accumulation of Ag(s)-NPs in the cells. Our libraries could distinctively differentiate the core (pink color) and shell (yellow color) clusters of Ag(s)-NPs. Once the pixel identity of Ag(s)-NP signature spectra was established, we randomly selected a pixel to study individual spectra after background subtraction (Fig. 2b; ESI Fig. 8†). We quantified spectra representing NPs in the cytoplasm or nucleus within single cells (Fig. 2c). It was apparent that our Ag(s)-NPs were dynamically moving in and out of the cells, as depicted in the fluctuation of total NPs in a single cell. The NPs were also moving in and out of the cell nucleus, as shown by the number of NPs in the nucleus at each time point. In this particular study, cells were also moving in or out from our field of view. More Ag(s)-NPs would eventually accumulate in the cells. Ag(s)-NPs would subsequently accumulate in the cell nucleus (ESI Fig. 7 and 8†).

We next studied time-lapse imaging of Au-NPs in single living cells (ESI Fig. 9a and 10†). We noted the continuous accumulation of Au-NPs in the cells. Once the pixel resembling the Au-NP spectral signature was identified, we randomly selected a pixel to study individual spectra after background subtraction (ESI Fig. 9b and 10†). Through the time-lapse imaging to detect the movements of Au-NPs, we could quantify potential NPs in the cytoplasm or nucleus within single cells (ESI Fig. 9c†). It was apparent that Au-NPs were dynamically moving in and out of the cells, as indicated by the fluctuation in total NPs in a single cell at a single time point. Similarly, NPs were in and out of the cell nucleus as depicted by the number of NPs in the nucleus at each time point. As time passed, more NPs accumulated in the cells, but this accumulation was started from the cytoplasm and followed by the nucleus. It was evident that Au-NPs preferentially localized in the cell nucleus (ESI Fig. 10 and 11†). While both Au-NPs and Ag(s)-NPs are largely known to localize in the nucleus,[25,26] we showed for the first time the dynamic movements of Au-NPs and Ag-NPs in the cytosol and nucleus (ESI Fig. 7 and 10†).

Electron microscopy and silver staining were used to verify the spectral imaging approach

To verify our subcellular localization findings of NPs in time-lapse imaging studies, we performed transmission electron microscopy (TEM) and silver staining analyses. TEM captured images of the cells treated with Ag(s)-NPs, Ag-NPs, and Au-NPs for 16 hours (Fig. 3a; ESI Fig. 12a†). While we were not able to capture the dynamics of these NPs due to sample fixation, the TEM studies confirmed the accumulation of NPs in the cell nucleus. Likewise, the localization of NPs was confirmed to be mostly in the nucleus of cells using silver staining to generate dark-brown contrast in phase images (Fig. 3b; ESI Fig. 12b†). Because the contrast was primarily enhanced by metallic silver attached at the periphery of the NPs, the spectral signatures within the NPs were not much altered (Fig. 3c; ESI Fig. 12c†).

Verification of the spectral imaging approach was performed *in vivo* using ICP-MS

We next assessed the practicality of spectral imaging to study the distribution of the NPs within mouse organ tissues. Remarkably, we found distribution of the Ag(s)-NPs, Ag-NPs and Au-NPs in the kidney, spleen, liver and heart tissues (Fig. 4a, ESI Fig. 13 and 14†). Importantly, the spectral characteristics of the core and shells of Ag(s)-NPs were not altered

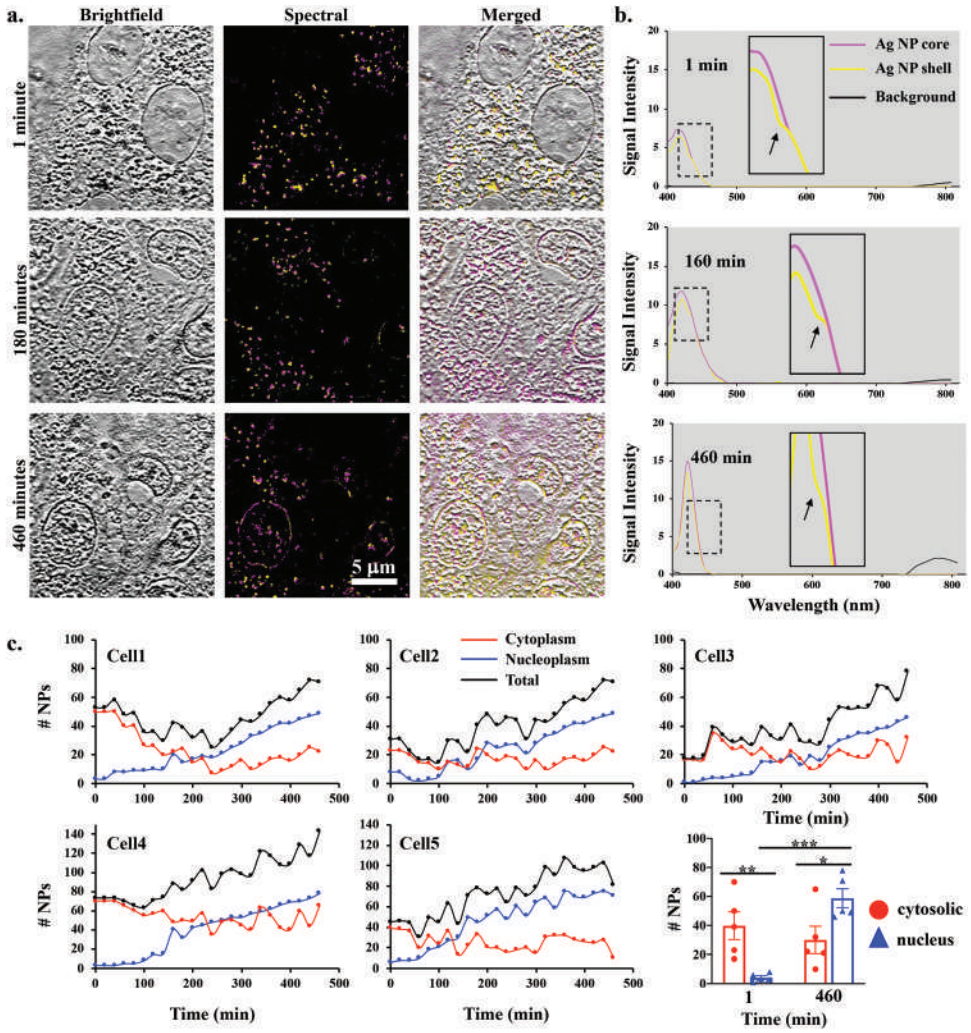

Fig. 2 Time-lapse imaging of Ag(s)-NPs. (a) Sequential time imaging of cells treated with 0.1 mg of Ag(s)-NPs in 2 mL media was captured for about 8 hours. Brightfield images and spectral scans were taken every 20 minutes (ESI Fig. 4†). (b) Spectral analysis was performed at the end of 8 hours after subtraction from the background spectra (ESI Fig. 5†). The Ag(s)-NP libraries differentiated the core and shell of NP clusters. The pink wavelength displays the intensity of the core area and the yellow wavelength shows the shell part (with a small shoulder; insert and arrow). (c) Line graphs illustrate the time-lapse analysis from 5 independent experiments. A number of Ag(s)-NPs (#NPs) was measured in one cell at each time point. Total #NPs were calculated from the localization of NPs in the cytoplasm (outside the nucleus) and nucleoplasm (inside the nucleus) within a cell. Comparisons were made at the beginning (1 min) and end (460 min) of the 8-hour experiments. $N = 5$. *, $P < 0.05$; **, $P < 0.01$; ***, $P < 0.001$.

(Fig. 4b and c). Based on our quantitative analyses, we showed that Ag(s)-NPs and Ag-NPs were distributed widely in the kidney and spleen, respectively (Fig. 5a). On the other hand, Au-NPs were in the liver (ESI Fig. 15a†). As a validation of NP distribution within the organs, we conducted ICP-MS analyses. Of note, the ICP-MS method and its standard curve did not differentiate between Ag(s)-NPs and Ag-NPs (ESI Fig. 15b†). We performed separate analyses of those tissues for Ag(s)-NPs, Ag-NPs or Au-NPs (Fig. 5b, ESI Fig. 15c†). We next examined the correlation analyses of the NP distribution. We found a significant correlation in the distributions of Ag(s)-NPs and Ag-NPs in spectral imaging and ICP-MS among the tissues (Fig. 5c). Likewise, a similar correlation was observed in Au-NPs (ESI Fig. 15d†), indicating a consistency between the spectral imaging and the ICP-MS approaches.

Discussion

The significance of the use of spectral imaging in our studies are as follows. First, we were able to identify and quantify the presence of NPs without the need to destroy or liquify the samples. This allowed us to perform live-cell imaging that was otherwise not possible. Second, we could calibrate the spectral library by using both imaging and the singularity/plurality of the spectral "signature" of a chemical. In Ag(s)-NPs, for example, we could observe the plurality of spectra at 420 nm, *i.e.* a peak with or without a shoulder. Looking at the images, we showed that the peaks without a shoulder were always at the center of NPs, whereas the peaks with a shoulder were localized at the periphery. Third, we did not need to fluorescently label our NPs. Labeling NPs required an additional step

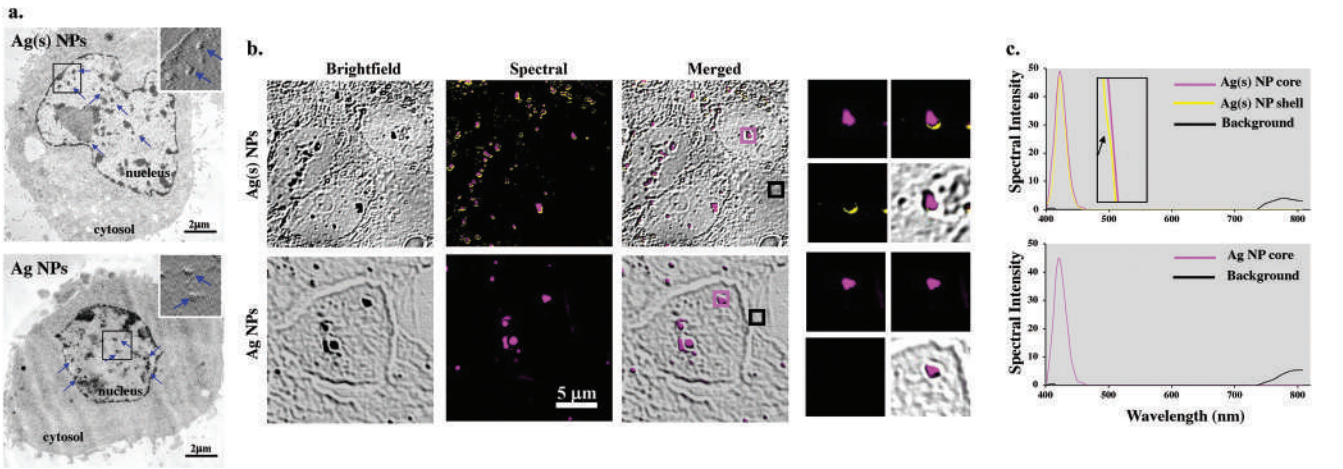

Fig. 3 TEM analysis and silver staining of Ag(s)-NPs and Ag-NPs. (a) TEM analyses were performed after treatment of Ag(s)-NPs or Ag-NPs for 16 hours. An embossing filter was applied in some regions of the cell nucleus for improving clarity of the NPs present (insert with arrows). (b) Cells after silver staining show brightfield images of the Ag(s)-NP and Ag-NP treated cells for 16 hours. The spectral images were extracted and pseudo-colored for the Ag(s)/Ag-NPs. Merged images revealed superimposed brightfield and spectral images to show the location of Ag(s)/Ag-NPs in the cell nucleus. The pink pseudocolor shows the core area of the Ag(s)/Ag-NPs, while the yellow color represents the shell region of Ag(s)-NPs. (c) The spectral graphs clarifying the wavelength peaks of Ag(s)/Ag-NPs at ~420 nm. The pink wavelength exhibits the intensity of the core area and the yellow wavelength displays the shell region. The black color shows the spectrum of the background area. *N* = 5.

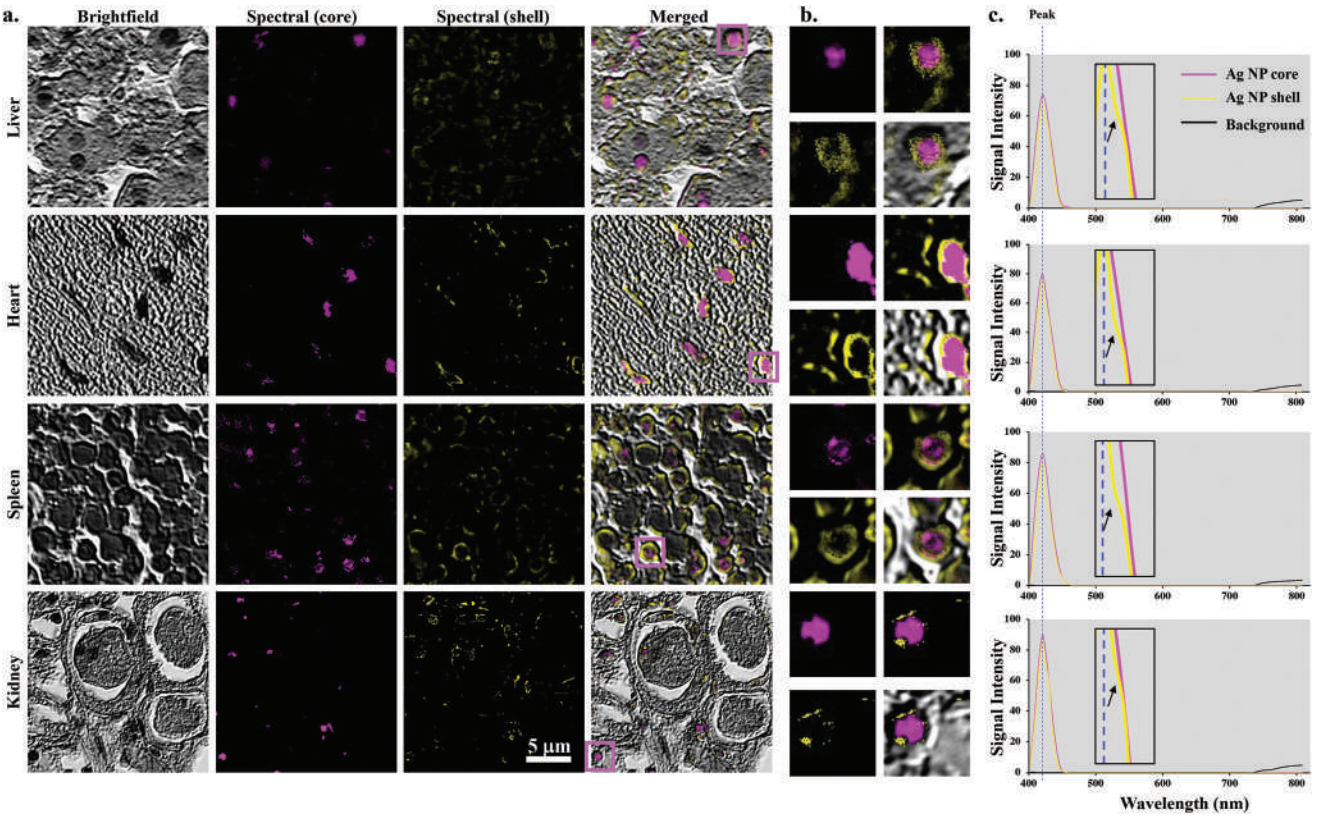

Fig. 4 Distribution of Ag(s)-NPs in animal tissues. (a) Brightfield images of the Ag(s)-NPs in different organ tissues (liver, heart, spleen, and kidneys) after intravenous injection with Ag(s)-NPs for 24 hours. The spectral images were extracted from the spectral libraries for Ag(s)-NPs. Merged images display combined brightfield and spectral images. (b) The pink pseudo-colored images show the core area of the Ag(s)-NPs, while the yellow color shows the shell region. (c) The graphs reveal the wavelength characteristics of the Ag(s)-NP cluster at ~420 nm. The pink wavelength exhibits the intensity of the core area and the yellow wavelength displays the shell part. The background is shown as a black colored wavelength. *N* = 5.

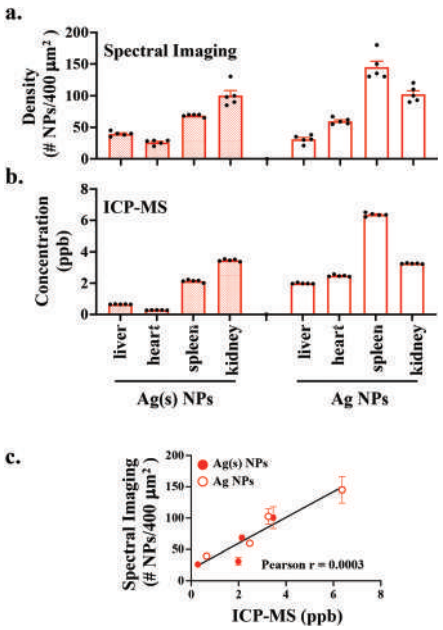

Fig. 5 Correlation analysis of Ag(s)-NP and Ag-NP distributions in the tissues using spectral imaging and ICP-MS. The bar graphs exhibit the distributions of Ag(s)-NPs and Ag-NPs in the liver, heart, spleen, kidneys, which were obtained using spectral imaging (a) or ICP-MS (b). (c) The correlation analysis of the distribution of Ag(s)-NPs and Ag-NPs in different organs between ICP-MS and spectral imaging is shown. N = 5 for each group and organs.

in the synthesis process, making the process more expensive and laborious. Labeled NPs could also alter the molecular functions and characteristics of NPs.[8–10] Fourth, spectral imaging was also applicable to fluorescent or auto-fluorescent molecules. Using spectral imaging, we were able to visualize fluorescent molecules fairly easily based mainly on their predominant fluorescence spectra (data not shown).[20] Note that the spectral identities might be different between non-labeled and fluorescent-labeled NPs. A fluorescence microscope might be more practical to detect the fluorescent-labeled NPs. Fifth, the spectral imaging approach was a simple yet inexpensive method for unlabeled NPs, the resolution of which depends on the quality of the lens and camera from standard optical microscopes. Unlike laser-based microscopic devices, such as in Raman spectroscopy, spectral imaging systems could be installed on upright or inverted microscopes that are readily available in many research laboratories.

Using spectral imaging, we were able to observe the dynamic uptake, movement, and distribution of different types of free-labeled NPs in a single cell. Conducting the live imaging technique while scanning the spectra from 400 to 800 nm, we were able to explore the behaviors of the NPs in a single cell, in which the NPs eventually accumulate in the cell nucleus. The spectral imaging was validated by both TEM and silver staining studies, although TEM and silver staining techniques did not provide the live-dynamics nature of NPs due to the requirement for cell fixation. In addition, we were able to study the distribution of NPs among tissues using spectral imaging. We found that Ag(s)-NPs and Ag-NPs were primarily localized in the kidneys and spleen, respectively. On the other hand, Au-NPs were distributed primarily in the liver. Of note, these tissues could be easily visualized with standard H&E staining, allowing easier sample preparation relative to an ICP-MS approach. It is known that larger nanoparticles (>6 nm) are cleared from the blood by the reticuloendothelial system. They accumulate in the liver and spleen; they are also captured by the mononuclear phagocyte system, which can be eliminated by the hepatobiliary system or may remain in the body for a long time.[27–29] However, it has been reported that the highest concentration of Ag-NPs is initially found in the liver, and over time the highest concentration of Ag-NPs should be found in the spleen.[30] Importantly, the spectral imaging was confirmed by the conventional ICP-MS technique with respect to tissue distribution analyses.

A few label-free methods have been developed for observing NPs in live cells. For example, transitory absorption microscopy has been utilized to capture carbon nanotubes in cells, and scatter-enhanced phase-contrast microscopy has been utilized to assess the intracellular behavior of unlabeled silicon nanowires.[15,31] Other approaches, such as hyperspectral stimulated Raman scattering microscopy,[13] optical diffraction tomography,[11] and dark-field microscopy,[32] have been utilized to investigate unlabeled NPs inside cells. However, using current technology to track unlabeled NPs in live cells in real-time with reliable spatial resolution remains a challenge. Besides, it is necessary to monitor both NPs and biomolecules to fully comprehend the interaction between NPs and cells/tissues. To the best of our knowledge, no technique has utilized a broader band of spectra in the range of 400–800 nm for real-time imaging of label-free NPs. A broader spectrum is required to extract more precise characteristics of a single molecule.[20] Specifically, this approach provides a more specific fingerprinting for each NP.

In summary, the combination of spectroscopy and imaging provides high-resolution spatial and temporal information of spectral characteristics in each pixel. This approach could serve as a valuable technique to understand the distribution, dynamic movement, and behavior of nanoparticles used in biomedical research and clinical medicine.

Conclusions

Spectral imaging provides both intensity and spectral information for each pixel of an image. We have achieved spectral resolution to 9 nm between 400 and 800 nm, resulting in 45 unique datapoints for each spectrum in each pixel. We have also integrated our image and spectral analyses by using artificial intelligence to recognize the datapoints by interconnecting each point to provide unique information of chemical fingerprints. This strategy allows differentiation between the core and the shell of silver-nanoparticles (Ag-NPs) for the first time. The advances of spectral imaging resolution and analysis also

allow us to detect the dynamics of NP distribution and tracking/identifying NPs and their subcellular localizations in single living cells. Without labeling the NPs and destroying the samples, the advanced spectral microscopy technique allows analyzing NPs in fixed cells, living cells and tissue samples *in vivo*.

Author contributions

QAA collected data, analyzed data and drafted the manuscript. RP and AKB synthesized and characterized the nanoparticles and helped design some studies. SOA contributed in the H&E and silver staining experiments (double-blind). AMN provided data, statistical analyses and improved interaction points in the software. NK participated in the spectral imaging system and software analysis. AMM analyzed the TEM images. SMN conceived the idea, designed research and oversaw the experimental progress. All authors were participating in finalizing the draft of the manuscript.

Notes

All animal procedures were performed in accordance with the Guidelines for Care and Use of Laboratory Animals of Chapman University. The Institutional Animal Care and Use Committee at Chapman University approved our animal studies, and our animal facility was approved by the Office of Laboratory Animal Welfare (OLAW). The OLAW assurance number is D17-00960.

Conflicts of interest

There are no conflicts of interest to declare.

Acknowledgements

This work was supported in part by the NIH HL131577 and HL131577-S1. The authors acknowledge the use of facilities and instrumentation at the UC Irvine Materials Research Institute (IMRI), which is supported in part by the National Science Foundation through the UC Irvine Materials Research Science and Engineering Center (DMR-2011967). The completion of this work by QAA partially fulfilled the requirements for her Ph.D. degree program in Biomedical and Pharmaceutical Sciences. At Chapman University, A. Sharma provided advice on the imaging validations, F. Amirrad assisted QAA in supervising the tissue processing training, and M. Takahashi and D. Larin-Henriquez were involved in mouse maintenance, reagent preparations and ordering. Li Xing at IMRI assisted in TEM studies.

References

1 D. C. Antonio, C. Cascio, D. Gilliland, A. J. Nogueira, F. Rossi and L. Calzolai, *Biointerphases*, 2016, **11**, 04B309.
2 D. Vanhecke, L. Rodriguez-Lorenzo, M. J. Clift, F. Blank, A. Petri-Fink and B. Rothen-Rutishauser, *Nanomedicine*, 2014, **9**, 1885–1900.
3 S. Lee, X. Bi, R. B. Reed, J. F. Ranville, P. Herckes and P. Westerhoff, *Environ. Sci. Technol.*, 2014, **48**, 10291–10300.
4 R. Pala, A. M. Mohieldin, R. T. Sherpa, S. H. Kathem, K. Shamloo, Z. Luan, J. Zhou, J. G. Zheng, A. Ahsan and S. M. Nauli, *ACS Nano*, 2019, **13**, 3555–3572.
5 R. Pala, A. M. Mohieldin, K. Shamloo, R. T. Sherpa, S. H. Kathem, J. Zhou, Z. Luan, J. G. Zheng, A. Ahsan and S. M. Nauli, *Nano Lett.*, 2019, **19**, 904–914.
6 G. S. Shekhawat and V. P. Dravid, *Science*, 2005, **310**, 89–92.
7 L. Tetard, A. Passian, K. T. Venmar, R. M. Lynch, B. H. Voy, G. Shekhawat, V. P. Dravid and T. Thundat, *Nat. Nanotechnol.*, 2008, **3**, 501–505.
8 S. Snipstad, S. Hak, H. Baghirov, E. Sulheim, Y. Morch, S. Lelu, E. von Haartman, M. Back, K. P. R. Nilsson, A. S. Klymchenko, C. de Lange Davies and A. K. O. Aslund, *Cytometry, Part A*, 2017, **91**, 760–766.
9 T. Tenuta, M. P. Monopoli, J. Kim, A. Salvati, K. A. Dawson, P. Sandin and I. Lynch, *PLoS One*, 2011, **6**, e25556.
10 C. Corbo, R. Molinaro, A. Parodi, N. E. Toledano Furman, F. Salvatore and E. Tasciotti, *Nanomedicine*, 2016, **11**, 81–100.
11 D. Kim, N. Oh, K. Kim, S. Lee, C. G. Pack, J. H. Park and Y. Park, *Methods*, 2018, **136**, 160–167.
12 F. Wang, B. Chen, B. Yan, Y. Yin, L. Hu, Y. Liang, M. Song and G. Jiang, *J. Am. Chem. Soc.*, 2019, **141**, 14043–14047.
13 B. Huang, S. Yan, L. Xiao, R. Ji, L. Yang, A. J. Miao and P. Wang, *Small*, 2018, **14**, 1–10.
14 G. L. C. Spicer, L. Almassalha, I. A. Martinez, R. Ellis, J. E. Chandler, S. Gladstein, D. Zhang, T. Q. Nguyen, S. Feder, H. Subramanian, R. de la Rica, S. A. Thompson and V. Backman, *Nanoscale*, 2018, **10**, 19125–19130.
15 J. F. Zimmerman, R. Parameswaran, G. Murray, Y. Wang, M. Burke and B. Tian, *Sci. Adv.*, 2016, **2**, e1601039.
16 L. Q. Chen, L. Fang, J. Ling, C. Z. Ding, B. Kang and C. Z. Huang, *Chem. Res. Toxicol.*, 2015, **28**, 501–509.
17 S. Patskovsky, E. Bergeron, D. Rioux and M. Meunier, *J. Biophotonics*, 2015, **8**, 401–407.
18 L. Q. Chen, S. J. Xiao, L. Peng, T. Wu, J. Ling, Y. F. Li and C. Z. Huang, *J. Phys. Chem. B*, 2010, **114**, 3655–3659.
19 J. Ling, Y. F. Li and C. Z. Huang, *Anal. Chem.*, 2009, **81**, 1707–1714.
20 Q. A. Alshammari, R. Pala, N. Katzir and S. M. Nauli, *Sci. Rep.*, 2021, **11**, 2703.
21 A. M. Fayaz, K. Balaji, M. Girilal, R. Yadav, P. T. Kalaichelvan and R. Venketesan, *Nanomedicine*, 2010, **6**, 103–109.
22 N. Claes, R. Asapu, N. Blommaerts, S. W. Verbruggen, S. Lenaerts and S. Bals, *Nanoscale*, 2018, **10**, 9186–9191.
23 E. Ertem, B. Gutt, F. Zuber, S. Allegri, B. Le Ouay, S. Mefti, K. Formentin, F. Stellacci and Q. Ren, *ACS Appl. Mater. Interfaces*, 2017, **9**, 34762–34772.

24 W. Haiss, N. T. Thanh, J. Aveyard and D. G. Fernig, *Anal. Chem.*, 2007, **79**, 4215–4221.
25 R. I. Berbeco, H. Korideck, W. Ngwa, R. Kumar, J. Patel, S. Sridhar, S. Johnson, B. D. Price, A. Kimmelman and G. M. Makrigiorgos, *Radiat. Res.*, 2012, **178**, 604–608.
26 P. V. Asharani, M. P. Hande and S. Valiyaveettil, *BMC Cell Biol.*, 2009, **10**, 65.
27 Y. N. Zhang, W. Poon, A. J. Tavares, I. D. McGilvray and W. C. W. Chan, *J. Controlled Release*, 2016, **240**, 332–348.
28 A. M. Alkilany and C. J. Murphy, *J. Nanopart. Res.*, 2010, **12**, 2313–2333.
29 M. Longmire, P. L. Choyke and H. Kobayashi, *Nanomedicine*, 2008, **3**, 703–717.
30 K. Dziendzikowska, J. Gromadzka-Ostrowska, A. Lankoff, M. Oczkowski, A. Krawczynska, J. Chwastowska, M. Sadowska-Bratek, E. Chajduk, M. Wojewodzka, M. Dusinska and M. Kruszewski, *J. Appl. Toxicol.*, 2012, **32**, 920–928.
31 L. Tong, Y. Liu, B. D. Dolash, Y. Jung, M. N. Slipchenko, D. E. Bergstrom and J. X. Cheng, *Nat. Nanotechnol.*, 2011, **7**, 56–61.
32 E. A. Gibbs-Flournoy, P. A. Bromberg, T. P. Hofer, J. M. Samet and R. M. Zucker, *Part. Fibre Toxicol.*, 2011, **8**, 2.

Electronic Supplementary Material (ESI) for Nanoscale.

SUPPLEMENT DATA

The use of advanced spectral imaging to reveal nanoparticle identity in the biological samples

Qamar A. Alshammari[*,1,2], Rajasekharreddy Pala[*,1], Ayan K. Barui[1], Saud O. Alshammari[1,3], Andromeda M Nauli[4], Nir Katzir[5], Ashraf M. Mohieldin[1], and Surya M. Nauli[1,6]

[*]Authors contribute equally
[1]Department of Biomedical & Pharmaceutical Sciences, Harry and Diane Rinker Health Science Campus, Chapman University, 9401 Jeronimo Road, Irvine, CA 92618-1908, USA
[2]Department of Pharmacology and Toxicology, Faculty of Pharmacy, Northern Border University, KSA.
[3]Department of Plant Chemistry and Natural Products, Faculty of Pharmacy, Northern Border University, KSA
[4]Department of Pharmaceutical Sciences, College of Pharmacy, Marshall B. Ketchum University, Fullerton, CA, USA.
[5]Applied Spectral Imaging, 5315 Avenida Encinas, Suite 150, Carlsbad, CA 92008.
[6]Department of Medicine, University of California Irvine, Irvine, CA 92868, USA.

Corresponding author:
Surya M. Nauli
Chapman University
University of California Irvine
9401 Jeronimo Road.
Irvine, CA 92618-1908
Tel: 714-516-5480
Fax: 714-516-5481
Email: nauli@chapman.edu; snauli@uci.edu

Supplement Figure 1

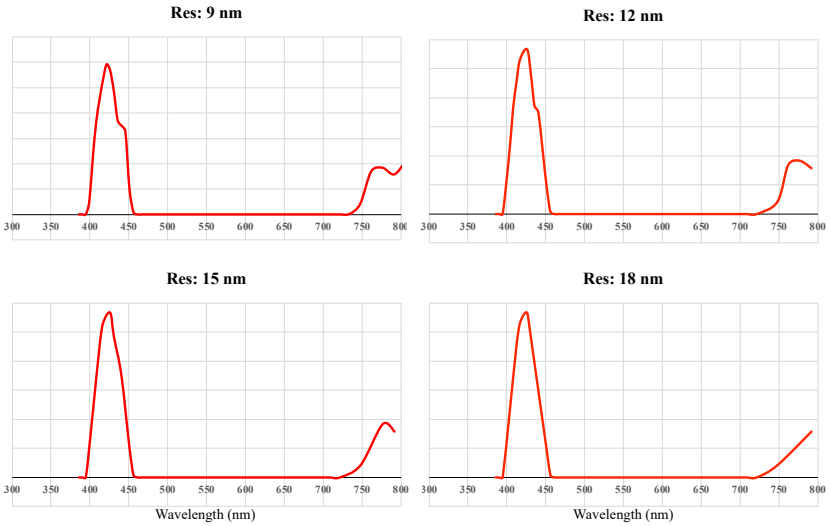

Supp Fig 1. An improved resolution of spectra imaging.
The shell of Ag-NPs was captured using spectral imaging at various resolutions (Res) of 9, 12, 15 and 18 nm. As resolution improves, more detailed changes can be analyzed to further refine the accuracy of the image analysis. A resolution of 9 nm was used throughout our studies.

Supplement Figure 2

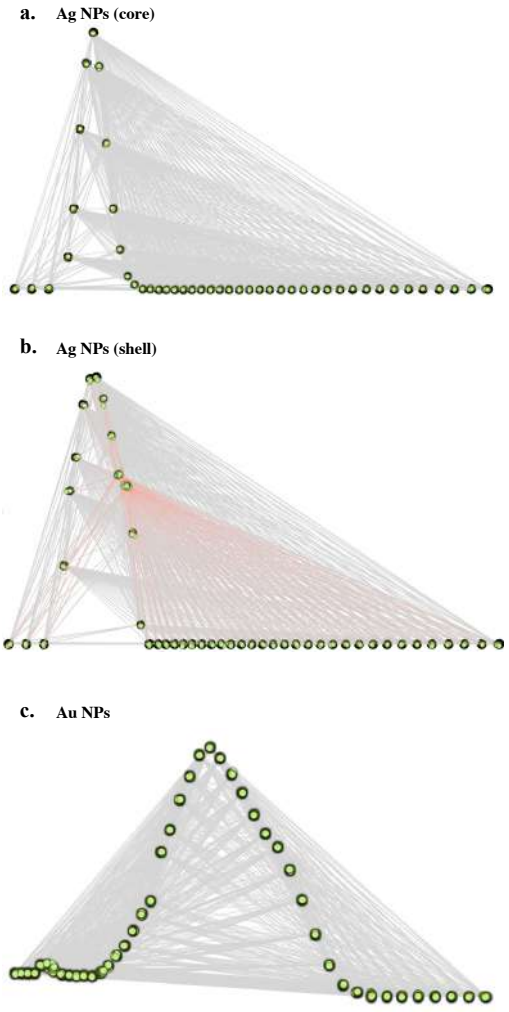

Supp Fig 2. A robust and rigorous analyses of spectra points
The identity (fingerprinting) of a molecule is analyzed based on the relative interactions among 45 spectral points for the core of Ag NPs (**a**), shell of Ag NPs (**b**) and Au NPs (**c**). These 45 points were generated from a spectral resolution of less than 10 nm between 400 nm and 800 nm. The 45 spectral points result in unique 990 interactions as indicated in the gray-color lines. Recognition artificial intelligence is used to improve spectral analysis by studying these unique interactions. As such, our analysis is able to specifically recognize about 90 distinct interactions to differentiate between core and shell of Ag NPs as indicated in the red-color lines.

Supplement Figure 3

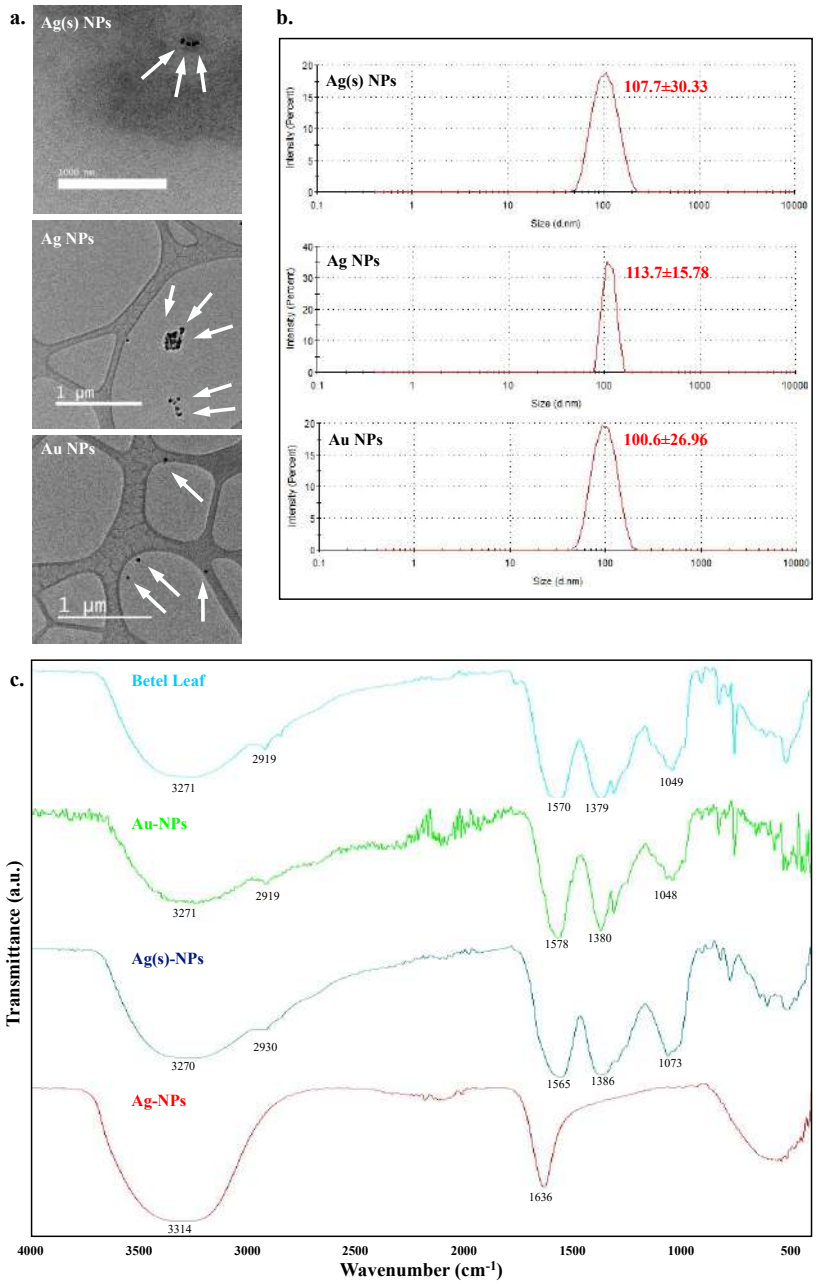

Supp Fig 3. Characterizations of different types of NPs
(a) The white arrows point to nanoparticles (NPs). (**b**) Dynamic light scattering shows the size of NPs (hydrodynamic diameter in nm; d). (**c**). Spectra taken from Fourier-transform infrared spectroscopy reveal key peaks representing polyphenols (O-H stretching; aromatic C-C=C stretching), carboxylic acids (O-H bending), protein molecules (N-H stretching; N-H bending) and H-O-H scissor of water molecules. Please see Method for details.

Supplement Figure 4

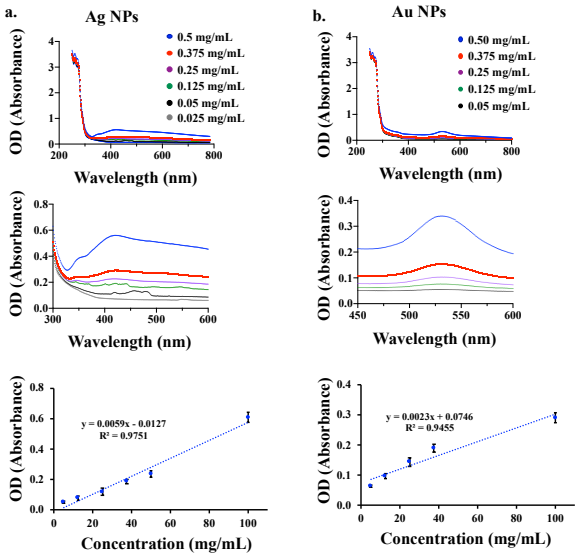

Supp Fig 4. UV-VIS spectra of Au-NPs **(a)** and Ag(s)-NPs **(b)** with maximum wavelengths at 536 and 420 nm, respectively. Different lines represent different concentrations. The middle panels present the magnified areas of NPs peaks. The lower panels show linear regression analysis of the corresponding peaks of Au-NPs and Ag(s)-NPs at different concentrations.

Supplement Figure 5

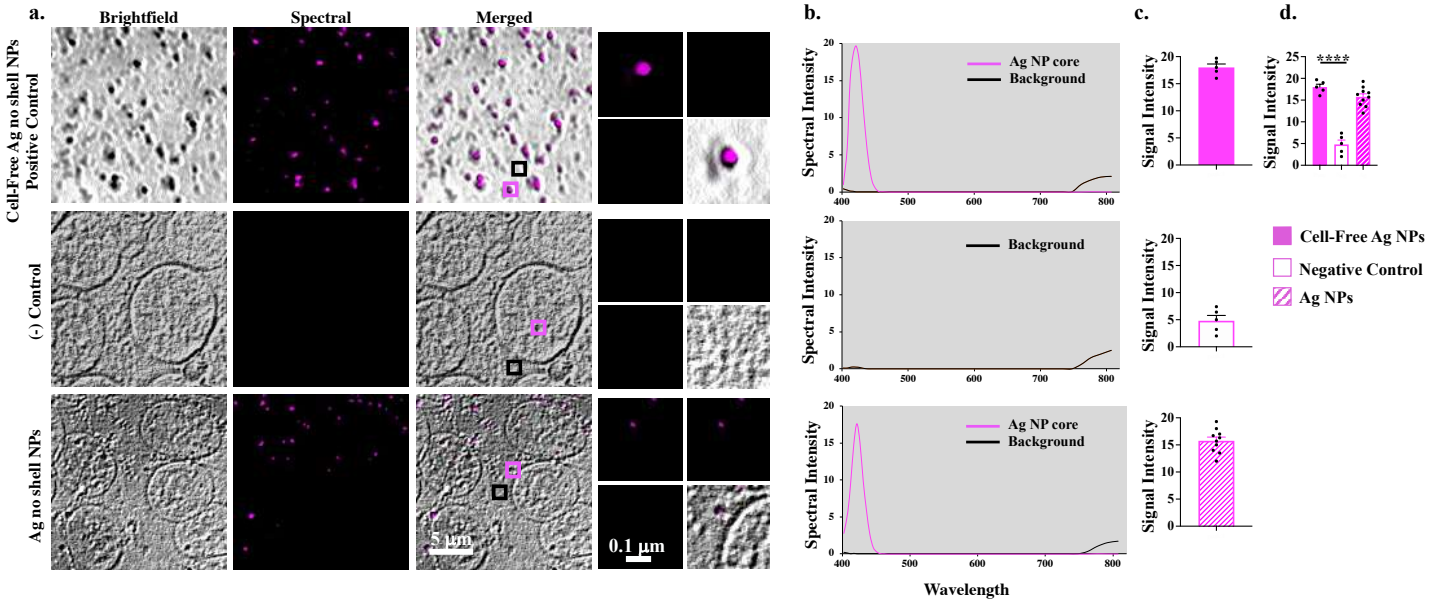

Supp Fig 5. Identification of Ag-NPs spectra
(a) Brightfield images are shown for Ag-NPs in the cell-free system (positive control), fixed cells (negative control), and 16-hour Ag-NPs-treated cells. The pseudo-colored spectral images were extracted from the spectra library for the Ag-NPs. Merged images exemplify superimposed brightfield and spectral images. The pink spectral image exhibits the core area of the Ag-NPs. **(b)** The graphs demonstrate the wavelength peaks of Ag-NPs clusters at ~420 nm for the positive control and the incubated cells. The pink wavelength presents the intensity of the core area. The black color displays the spectrum of the background area. The negative control spectra were identified based on unmatched spectra from our libraries. **(c)** The bar graphs show the variation of intensity data points at 420 nm. **(d)** The signal intensities were compared among cell-free positive control, non-treated cells negative control, and Ag-NPs-treated cells. N=4-5 for each positive and negative controls; N=8 for experimental groups. ****, P<0.0001.

Supplement Figure 6

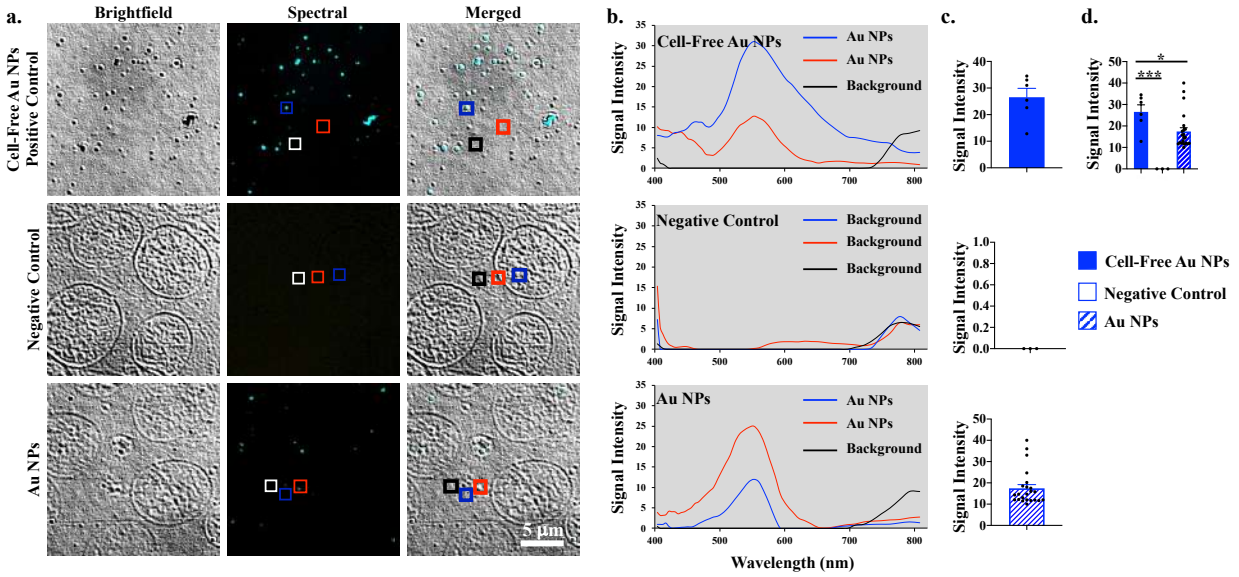

Supp Fig 6. Identification of Au-NPs spectra

(a) Brightfield images are shown for Au-NPs in the cell-free system (positive control), fixed cells (negative control), and 16-hour Au-NPs-treated cells. The pseudo-colored spectral images were extracted from the spectra libraries for Au-NPs. Merged images show combined brightfield and spectral images. **(b)** The graphs show the wavelength characteristics of the Au-NPs cluster at ~552 nm for the positive control and with cell incubation. Au-NPs graphs were shown after an automatic background subtraction by the software (**See Method**). The blue line displayed the area that contains higher wavelength intensity, and the red showed the region with less intensity. The background exhibited as a black color wavelength. The negative control graph shows the wavelengths. The negative control spectra were identified based on unmatched spectra from our libraries. **(c)** The bar graphs present the variation of intensity data points of the Au-NPs cluster peak of 552 nm. **(d)** The signal intensities were compared among cell-free positive control, non-treated cells negative control, and Au-NPs-treated cells. N=6 for each positive and negative controls; N=24 for experimental groups. *, P<0.05; ***, P<0.001.

Supplement Figure 7

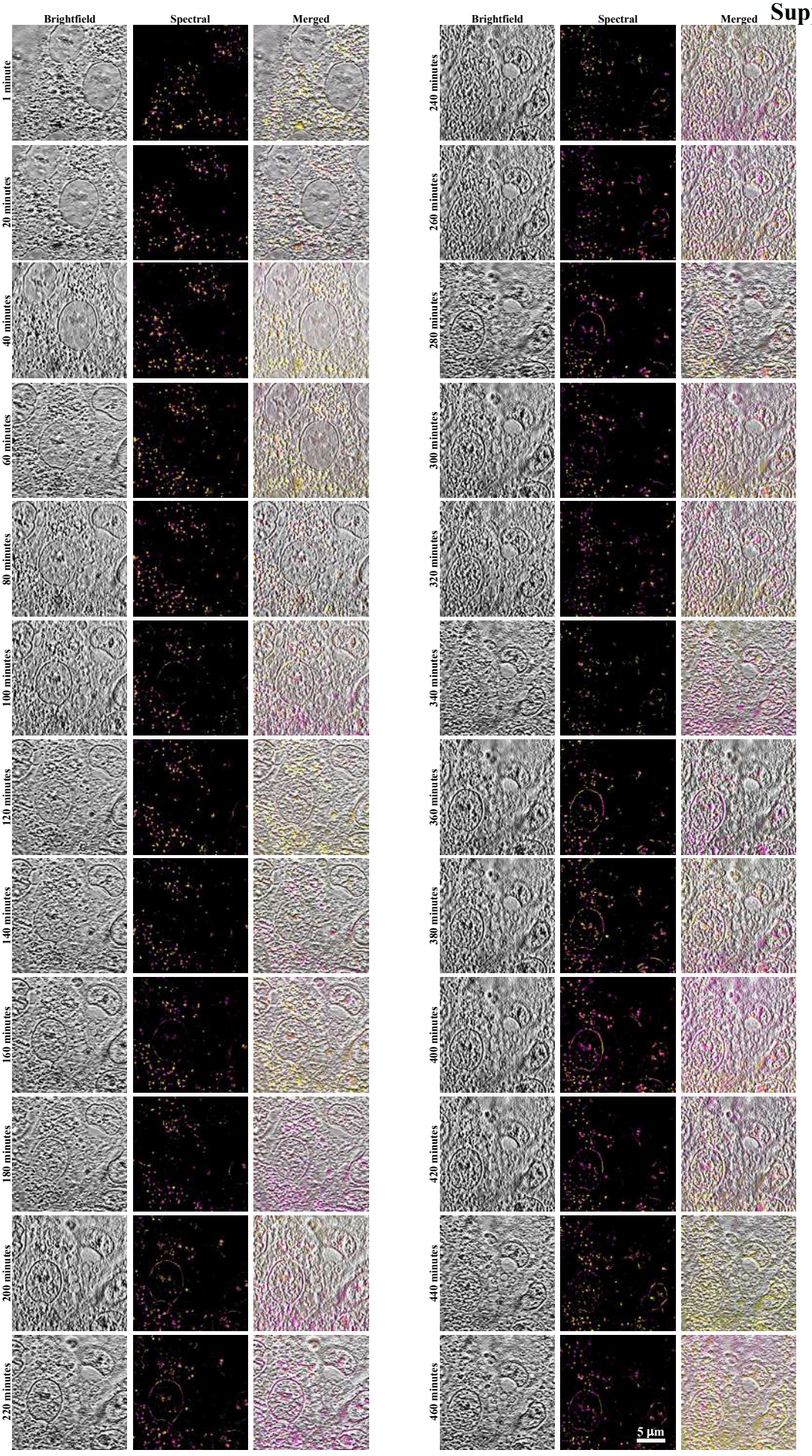

Supp Fig 7. Time-lapse imaging for the cells treated with 0.1 mg of Ag(s)-NPs in 2mL media. Images were captured every 20 minutes for about 8 hours. Over time, the number of Ag(s)-NPs increases in the nucleoplasm area.

Supplement Figure 8

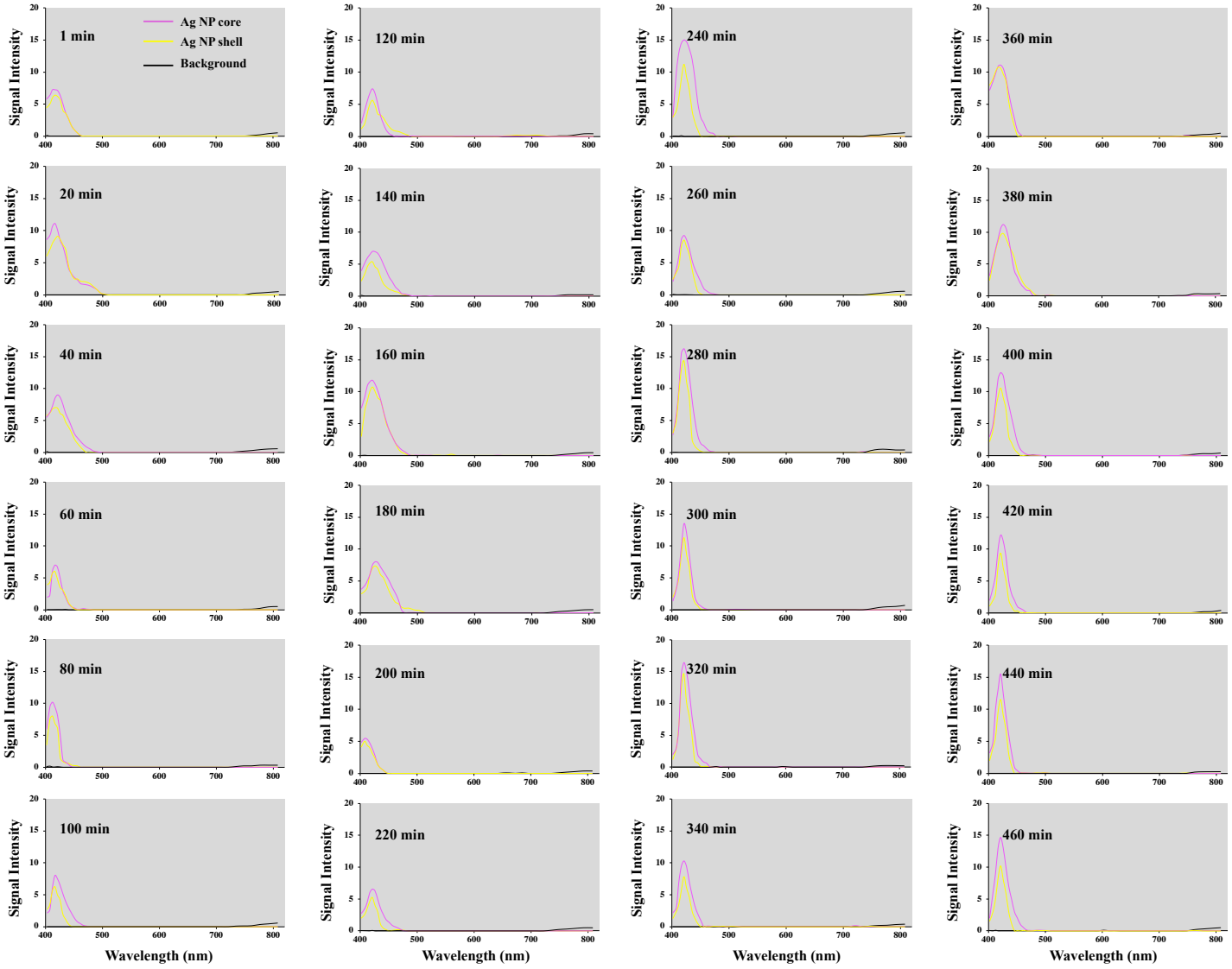

Supp Fig 8. Different graphs represent different Ag(s)-NP wavelengths. The pink lines represent the core area of Ag(s)-NPs, while the yellow lines show the shell of Ag(s)-NPs. The black lines represent the background area.

Supplement Figure 9

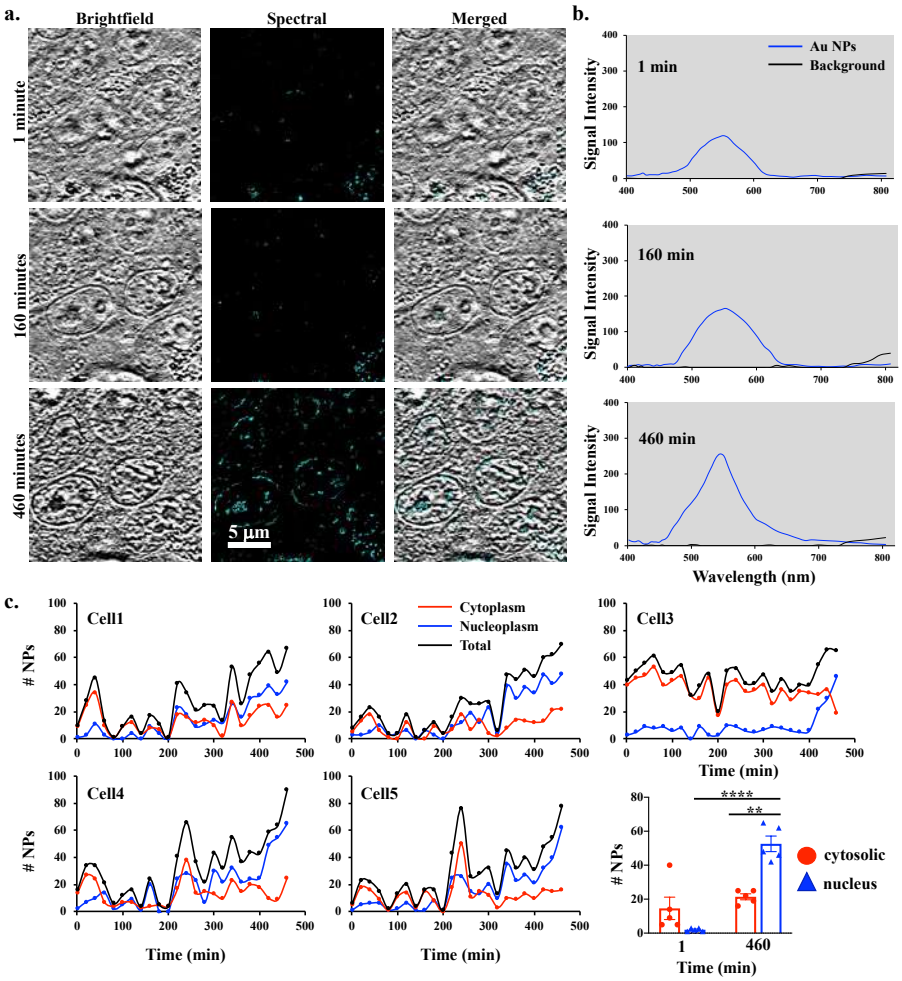

Supp Fig 9. (a) Sequential time imaging of cells treated with Au-NPs was captured for about 8 hours. Brightfield image and spectral scan were taken at every 20 minutes (**Supp Fig. 7**). **(b)** Spectral analysis was performed at the end of 8 hours after subtraction from the background spectra (**Supp Fig. 8**). **(c)** Line graphs illustrate the time-lapse analysis from 5 independent experiments. Number of Au-NPs (#NPs) was measured in one cell at each time point. Total #NPs were calculated from localization NPs in cytoplasm (outside nucleus) and nucleoplasm (inside nucleus) within a cell. Comparisons were done at the beginning (1 min) and end (460 min) of the 8-hour experiments. N=5. **, P<0.01; ****, P<0.0001.

Supplement Figure 10

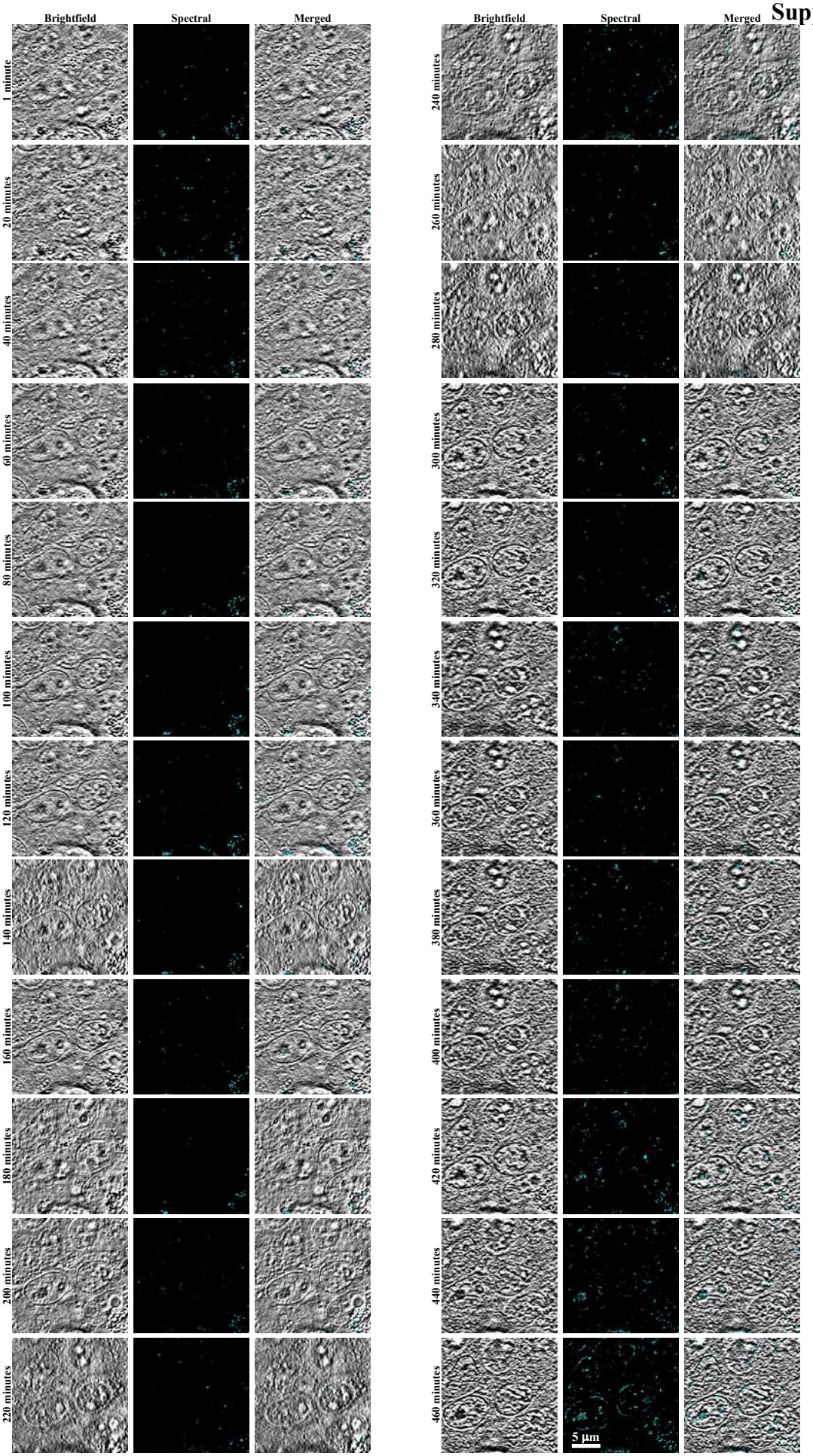

Supp Fig 10. Time-lapse imaging for the cells treated with Au-NPs. Images were captured every 20 minutes for 7 hours and 40 minutes. Over time, the number of Au-NPs increased in the nucleoplasm area.

Supplement Figure 11

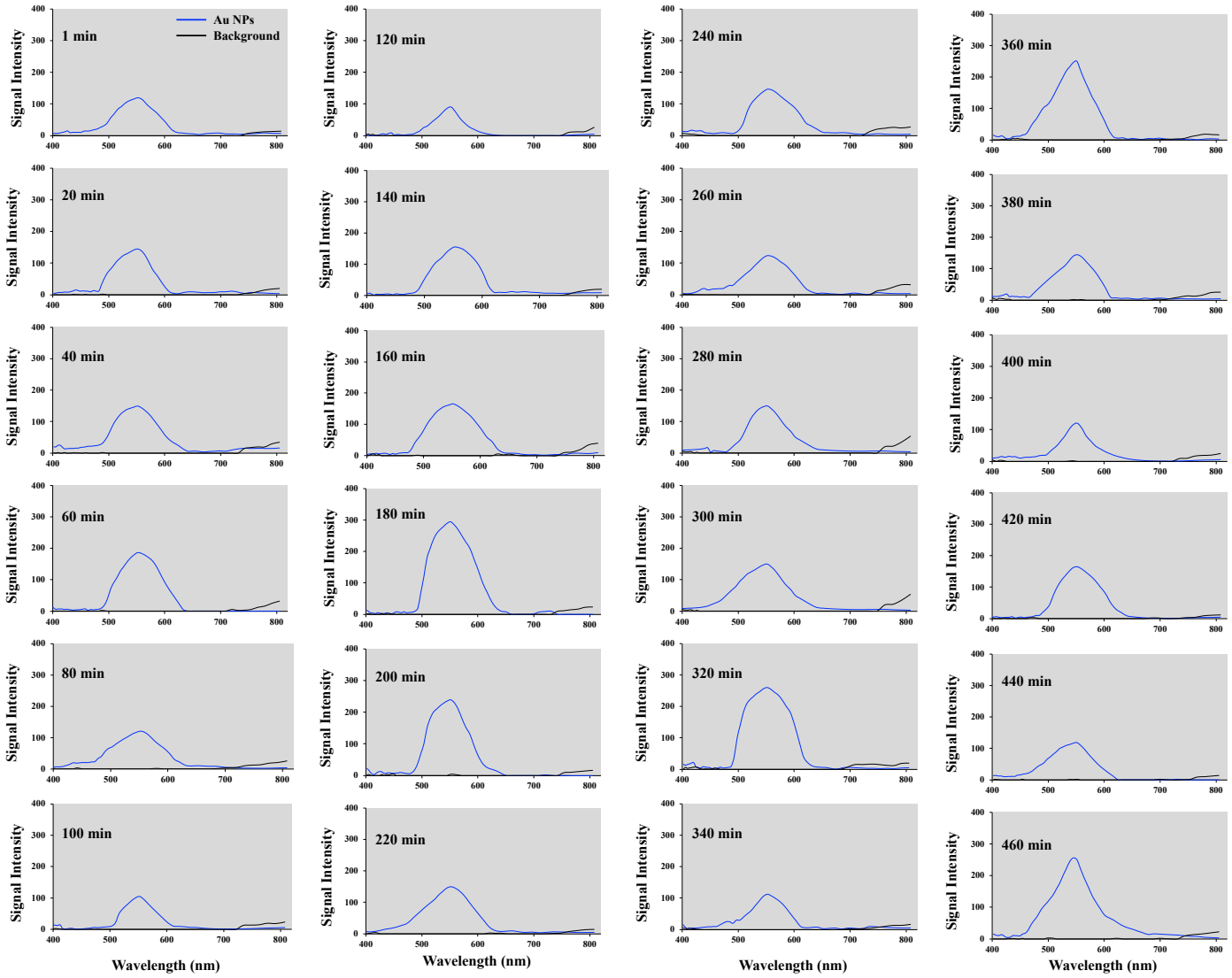

Supp Fig 11. Different graphs represent different Au-NPs cluster wavelengths with blue color, while black color exemplifies the background area.

Supplement Figure 12

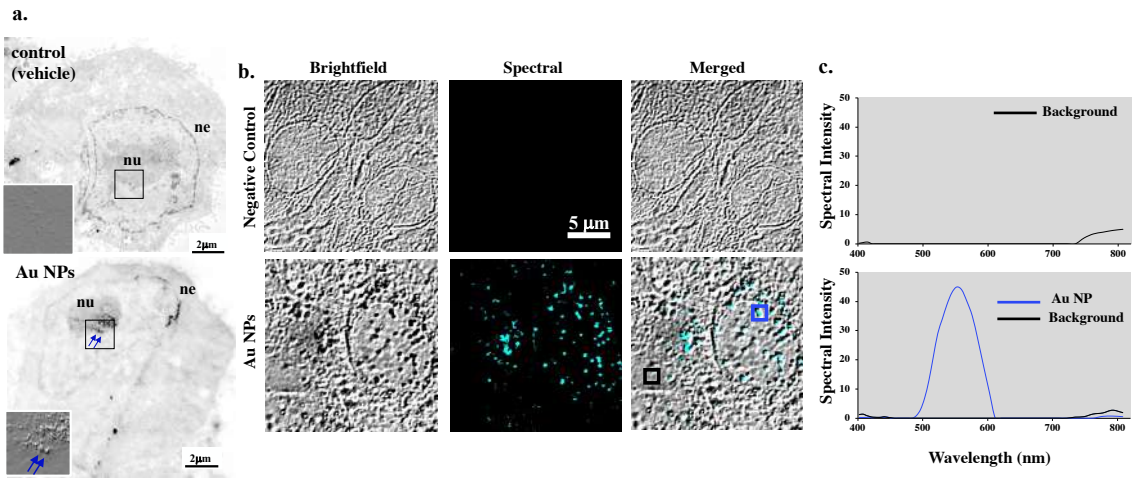

Supp Fig 12. (a) TEM analyses were performed after treatment of saline (control) or Au-NPs for 16 hours. An embossing filter was applied in some regions of cell nucleus for better clarity of the presence of NPs (insert with arrows). nu=nucleolus; ne=nuclear envelop. **(b)** Brightfield images of the silver stained non-treated (control) or 16 hours Au-NPs treated cells. The spectral images were extracted and pseudo-colored for the Au-NPs. Merged images revealed superimposed brightfield and spectral images to show the location of Au-NPs in the cell nucleus. **(c)** The spectral graphs clarify the wavelength peaks of Au-NPs at ~552 nm. N=5.

Supplement Figure 13

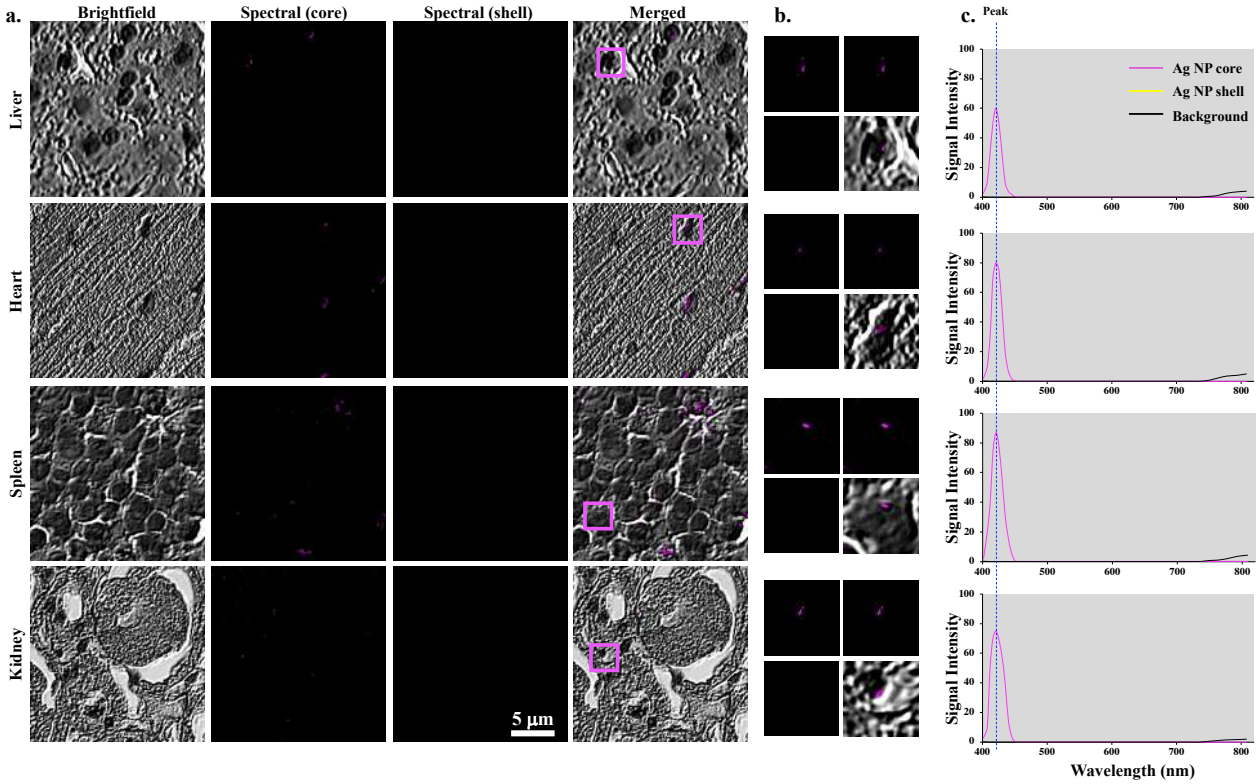

Supp Fig 13. (a) Brightfield images of the Ag-NPs in different organs tissues (liver, heart, spleen kidney) after intravenous injection of Ag-NPs for 24 hours. The spectral images were extracted from the spectra libraries for Ag-NPs. Merged images display combined brightfield and spectral images. **(b)** The Ag-NPs were shown in the pink pseudo-colored images. **(c)** The graphs reveal the wavelength characteristics of the Ag-NPs cluster at ~420 nm. The pink wavelength exhibits the intensity of the core area; the yellow wavelength displays the shell part. The background is shown as a black color wavelength. N=5.

Supplement Figure 14

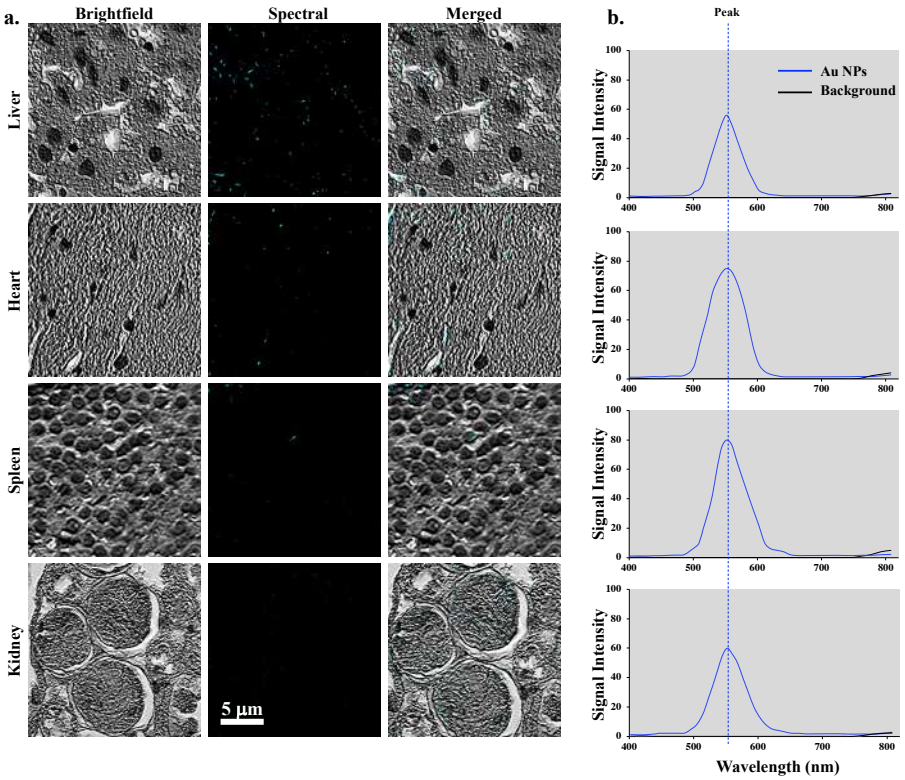

Supp Fig 14. (a) Brightfield images of the Au-NPs in different organs tissues (liver, heart, spleen kidney) after intravenous injection of Au-NPs for 24 hours. The spectral images were extracted from the spectra libraries for Au-NPs. Merged images display combined brightfield and spectral images. **(b)** The graphs reveal the wavelength characteristics of the Au-NPs at ~552 nm. The blue wavelength exhibits Au-NPs. The background is shown as a black color wavelength. N=5.

Supplement Figure 15

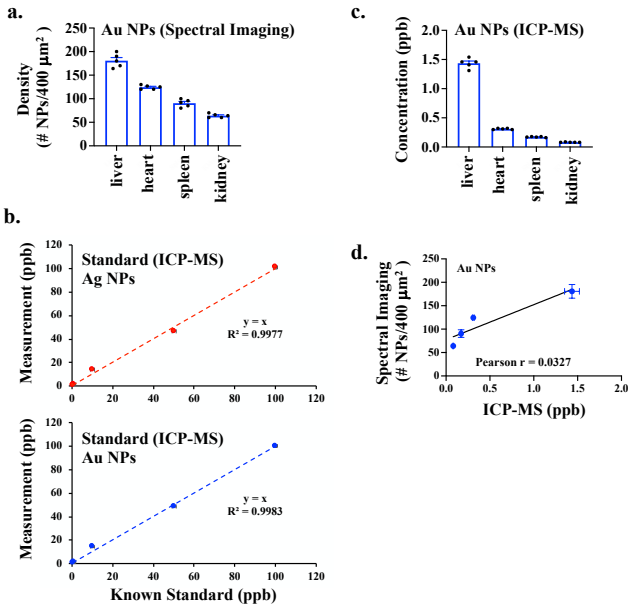

Supp Fig 15. (a) Tissue distribution of Au-NPs by spectral imaging is summarized in the bar graph. **(b)** Representative standard curves for ICP-MS are shown for Ag(s)-NPs and Au-NPs (0.5 to 100 ppb). **(c)** Tissue distribution of Au-NPs by ICP-MS is summarized in the bar graph. **(d)** The correlation analysis of the distribution of Au-NPs in different organs between ICP-MS and spectral imaging was performed. N=5 for each group.

SUPPLEMENT METHODS

The use of advanced spectral imaging to reveal nanoparticle identity in the biological samples

Qamar A. Alshammari[*,1,2], Rajasekharreddy Pala[*,1], Ayan K. Barui[1], Saud O. Alshammari[1,3], Andromeda M Nauli[4], Nir Katzir[5], Ashraf M. Mohieldin[1], and Surya M. Nauli[1,6]

[*]Authors contribute equally
[1]Department of Biomedical & Pharmaceutical Sciences, Harry and Diane Rinker Health Science Campus, Chapman University, 9401 Jeronimo Road, Irvine, CA 92618-1908, USA
[2]Department of Pharmacology and Toxicology, Faculty of Pharmacy, Northern Border University, KSA.
[3]Department of Plant Chemistry and Natural Products, Faculty of Pharmacy, Northern Border University, KSA
[4]Department of Pharmaceutical Sciences, College of Pharmacy, Marshall B. Ketchum University, Fullerton, CA, USA.
[5]Applied Spectral Imaging, 5315 Avenida Encinas, Suite 150, Carlsbad, CA 92008.
[6]Department of Medicine, University of California Irvine, Irvine, CA 92868, USA.

Corresponding author:
Surya M. Nauli
Chapman University
University of California Irvine
9401 Jeronimo Road.
Irvine, CA 92618-1908
Tel: 714-516-5480
Fax: 714-516-5481
Email: nauli@chapman.edu; snauli@uci.edu

Materials and Methods

Materials. LL-CPK1 (ATCC® CL101.1TM) porcine renal epithelial cells from proximal tubule were purchased from American Type Culture Collection (ATCC; Manassas, VA). Trypsin, penicillin-streptomycin solution (lot# 04619001), phosphate-buffered saline (PBS; lot# 05319001), and Dulbecco's Modified Eagle Medium (DMEM) (lot# 20818006) were purchased from Corning (Manassas, VA). Fetal bovine serum (FBS) was obtained from Seradigm (Logan, UT), paraformaldehyde (PFA) from Electron Microscopy Services (Hatfield, PA), Mounting Media HistoChoice® from Amresco, lysis buffer from Thermo scientific (Rockford, IL), protease inhibitor cocktail from Roche (Mannheim, Germany), Nitric Acid TraceMetal Grade (lot# 1119040) and Hydrochloric Acid TraceMetal Grade (lot# 4119080) from Fisher Scientific (Fair Lawn, NJ 07410), and Silver Staining Kit from Invitrogen (Cat no. LC6070).

Cell culture. LL-CPK1 cells were cultured to a confluent monolayer in DMEM supplemented with 10% FBS and 1% penicillin-streptomycin at 37°C in 5% CO_2 and 95% humidity. Cells were trypsinized (using a 0.05% solution of trypsin) regularly for passage when 70-90% confluence was reached. For our experiments, cells were cultured to reach confluence before treatment with vehicle or different types of NPs.

Synthesis of Ag-NPs and Au-NPs. For the synthesis of Ag(s)-NPs, silver nitrate ($AgNO_3$) and for gold nanoparticles (Au-NPs), chloroauric acid ($HAuCl_4$) were purchased from Millipore-Sigma, USA and was used without further purification. Ag and Au-NPs synthesis were carried out by taking 5 mL of betel leaf broth (*Piper betle* L.) and adding 90 mL of 1×10^{-3} M aqueous $AgNO_3$ and $HAuCl_4$ solutions individually at room temperature, followed by exposing the reaction mixtures to direct sunlight irradiation at Chapman University School of Pharmacy, CA, USA (latitude 33°N) in June 2019 from the time period between 11:00 a.m. and 2:00 p.m. under clear sky conditions with different time periods ranging from 5 min to 1 h. The Ag and Au-NPs colloidal solutions thus obtained were purified by repeated centrifugation (by using a Thermofisher ultra microcentrifuge) at 20,000 rpm for 10 min followed by redispersion of the pellets of Ag and Au-NPs into 20 mL of ultrapure water. To further purify the NPs, the centrifuging and redispersion process was repeated for five times. The bio-reduction of the Ag and Au ions in solutions were monitored by periodic sampling of aliquots of the reaction mixtures and measuring the UV–vis spectrum of the solutions individually. Silver nanoparticles (no-shell) were also synthesized by chemical methods in order to compare with silver (core-shell NPs). Briefly, Ag NPs (no-shell) were prepared by reducing 180 mL of $AgNO_3$ (1×10^{-3} M) using 20 mL of $NaBH_4$ (0.04 mg/mL). The loose dark pellet was collected from chemically synthesizing Ag NPs through centrifugation at 20,000 rpm at 26 °C for 20 min in a Thermo ultra-microcentrifuge. The chemically synthesized Ag NPs were further purified by the centrifuging and redispersion process was repeated for three times.

UV-VIS Spectrum Detection. Spectrophotometer (SpectraMax M5 Microplate Reader) was used to read the ultraviolet-visible (UV-VIS). The UV-VIS wavelength of Ag-NP and Au-NP clusters were read at concentrations of 0.025, 0.05, 0.125, 0.25, 0.375, 0.5 mg/mL diluted in deionized water, which was filtered through Milli-Q (MilliporeSigma, Burlington, MA). The wavelength range of 200-800 nm was used to read the UV spectrum for all the chemicals.

DLS and FTIR. NP characterizations were carried as previously described[1, 2] (**Supp Fig. 3**). The DLS study exhibited broad distribution of particles for Au-NPs (100.6±27.0 nm) and Ag(s)-NPs (107.7±30.3 nm). This broad distribution of particles is often found for bio-synthesis of nanoparticles using plant extract. On the other hand, comparatively sharp distribution of particles was observed for chemically synthesized Ag-NPs (113.7±15.8 nm). The FTIR spectra revealed some evident peaks of Betel leaf extract at 3271 cm^{-1} (O-H stretching of alcohols and N-H stretching of amines), 2919 cm^{-1} (H-C-H stretching; aliphatic), 1570 cm^{-1} (aromatic C-C=C stretching and N-H bending of amides), 1379 cm^{-1} (O-H bending of carboxylic acids), and 1049 cm^{-1} (C-O stretching of esters). Similar peaks were also observed in the FTIR spectra of Au-NPs and Ag(s)-NPs. However, their peaks are slightly shifted in many cases in comparison with that of Betel leaf extract, which might be due to the interaction of nanoparticles with the phytochemicals of Betel leaf extract. The results overall indicate that different polyphenols (O-H stretching; aromatic C-C=C stretching), carboxylic acids (O-H bending) and protein molecules (N-H stretching; N-H bending) present in Betel leaf extract could be adsorbed on the surface of Au-NPs and Ag(s)-NPs during their synthesis, thereby stabilizing those nanoparticles. On the other hand, FTIR spectra of chemically synthesized Ag-NPs revealed peaks at 3314 cm^{-1} and 1636 cm^{-1} which can be assigned to O-H stretch and H-O-H scissor of water molecules (associated with Ag-NPs), respectively. Evidently, the FTIR spectra of biosynthesized Ag(s)-NPs and chemically synthesized Ag-NPs are completely different.

Cell Treatment. Cells were seeded on sterilized 22x22 mm coverslip (Globe Scientific), in 6 wells plate (Greiner bio-one Cellstar®, the total volume of 2 mL at each well) under normal growth conditions until reached 70-80% confluency. The cells then incubated with 100 µL of the selected chemical at different concentrations of NPs for 18 hrs. Then, the cells washed three times by PBS, fixed the cells for 10 min in fixing solution (2.5 mL PFA, 7.5 mL PBS and 0.2 g sucrose) at room temperature. Afterward, the coverslip was placed on the slide that contains 25 µL of Mounting Media overnight at room temperature.

Spectral Imaging. Spectral imaging instrument (Applied Spectral Imaging's GenASIs™ Hyperspectral Imaging System) and Olympus microscope (Model BX61) were used in this research. Images were manually acquired with 60X magnification objective. Xenon arc lamp was used as our light source in transmission mode through the sample. Contrast was produced through the absorption of light in dense areas of the sample. Ag-NPs and Au-NPs cluster wavelengths were identified by utilizing the brightfield filter. Optical Density (OD) spectra were extracted and used to view and classify spectra.

Our system used a previously described standard microscopy set-up[3]. This set-up was widely available in most laboratories. Hyperspectral system was based on a Sagnac interferometer. The beam splitter split the light originating from the selected area in the sample into two beams. A set of mirrors led the beams down two paths of various lengths. At the end of the paths, the two beams are combined and superimposed on the sensor. The total intensity of these two superimposed beams at each point of the sensor is a function of the spectrum of this point on the sample and the difference in the distance between the two paths. This difference is called the Optical Path Difference (OPD). The intensity of the merged beams is captured by a Charged-Coupled Device (CCD) camera. Each measurement is called a frame, which is a gray level image measured by the CCD camera. To extract a hyperspectral image a set of frames are acquired, each corresponds to

slightly different OPD. This process arose simultaneously for all pixels in the image. The vector of intensities at each pixel, collected from the set of images with shifted OPD's, is called an interferogram. The Hyperspectral image is derived by Fourier Transformation of the interferograms of all pixel.

For each NP type, we defined wavelengths, which represent areas that we selected within the image in order to compare their spectra and to build a spectral library after background subtraction. For instance, inside the chemical image, to compare the chemical substance spectrum with the background spectrum, we defined wavelengths in the area that contained NP clusters, and in the area that contains nothing (background). This background wavelength also represented an empty cover treated the same way but without the addition of NPs. We then displayed the two spectra (NPs and background). The NP spectra were obtained by subtracting the background spectra. After that, we saved these NP spectra in libraries for further cell analysis. At least 10 images were captured randomly from the cells that were treated with NPs. Afterward, we analyzed the captured images by using spectral libraries of the NPs and scanned all the areas to obtain the location that only matched with the NP libraries. For the Ag-NPs and Au-NPs samples, we used the brightfield SUN analysis (within the SpectraView software, Applied Spectral Imaging), which performs Spectral UNmixing, separating an image into layers that corresponded to the absorption spectra (libraries). This led us to quantify the amount and pinpoint the location of material according to its absorption spectra.

At a resolution of 9 nm (**Supp Fig. 1**), we were able to collect 45 unique datapoints for each spectrum in each pixel of an image. Each of the datapoint was converted to a binary value, and it thus contained 2 sets of information; wavelength-intensity for a human operator and relative-position for the computer analysis (**Supp Fig. 2**). To generate self-validation on the analysis, confirmation was acquired among those 45 points; each point self-validated toward the rest of 44 other points. This resulted in 990 unique interactions (${}_2C_{45}$). If this self-validation did not produce a confidence coefficient of 99%, the system will generate the next levels of interactions (${}_2C_{990}$, ${}_2C_{489,555}$, ${}_2C_{119,831,804,235}$, etc.). The analysis was incredible accurate at 99.99% when 10 spectral libraries or more were used.

Time-lapse imaging. LLCPK cells were grown on six wells plate and treated with 0.1 mg NPs in 2 mL media. Living cells were imaged using a spectral imaging system, every 20 minutes for 8 hrs.

Transmission Electron Microscopy. The cells were treated with Ag-NPs and Au-NPs and incubated for 18 hours. Afterward, the cells were washed three times for 5 minutes with PBS. Then, the cells were trypsinized and fixed for 60 min in primary fixation (2% paraformaldehyde and 2.5% glutaraldehyde in 1% PBS buffer) at room temperature, followed by three washing with PBS. The resulting samples were postfixed with 1% osmium tetroxide for 60 min, followed by three-time washing with buffer and three-time washing with water. Afterward, the cells were dehydrated in a series of alcohol, then embedded in epoxy resin. Ultrathin sections of 120 nm were then stained with uranyl acetate and lead citrate and observed by TEM. The slices were examined under a JEM-2100F transmission microscope (JEOL) and the images were recorded on Gatan Oneview CCD as an image montage with the aid of SerialEM software. For TEM image, the

microscope was operated at 200kV and the images were taken at a minimum magnification of 10,000.

Animal Studies. All animal procedures were performed according to Chapman University Animal Care and Use Committee Guidelines. A total of four groups of mice were injected intravenously with saline solution (vehicle control), Ag(s)-NPs, Ag-NPs or Au-NPs for a total treatment time of 24 hours. The total NPs were injected at 1 mg/kg in 45-days old wild-type C57BL6 Black with averaged body weight of 27.5±2.8 g. Both male and female mice were used and randomly selected for the treatments. Then, the mice were euthanized to collect liver, kidney, liver, heart, and spleen. Tissues were taken for spectral imaging or ICP-MS analyses.

ICP-MS measurement. Approximately 0.1 g of tissue (liver, kidney, heart, and spleen) weighed and added into 5 mL a mixture of concentrated nitric acid (HNO_3) and hydrochloric acid (HCl) (4: 1) in digestion vessels. All the vessels were immediately shaken by hand and covered overnight for pre-dissolution. Afterward, the vessels were placed in oil and heated to about 100 °C for around 3 hours. The Au samples were diluted with 1% (v/v) HNO3 and 1% (v/v) HCl; and the Ag and Ag (s) samples with 1% HNO3.

Measurement with ICP-MS. All prepared standards and tissue samples were measured by the ICP-MS system (Thermo Scientific iCAP RQ ICP-MS). Quantification was carried out within elements (100-0.5 ppb) internal standard correction. The main operating conditions for ICP-MS were as follows: the radio frequency (RF) power 1550 W; argon gas flow rates for the plasma, auxiliary, and nebulizer flow were 14 L min^{-1}, 0.8 L min^{-1}, and 1.07 L min^{-1}, respectively.

Hematoxylin and eosin staining. The tissue processing of the organs was performed by STP 120 Spin Tissue Processor (Thermo Fisher Scientific, USA). The dehydration step was performed by immersing the organs in a series of alcohol, 70% for 30 minutes, 80% for 30 minutes, 95% for 45 minutes, and 100% for 45 minutes. The clearing step was performed for 1.5 hours by using xylene. The last step of processing was the infiltration by paraffin for 1.5 hours. The tissues were then sectioned for H&E staining and observed under spectral imaging (**Table 1**).

Table 1. H&E staining steps

Compound	**Time**
Xylene	17 min
100% Ethanol	2 min
90% Ethanol	1 min
75% Ethanol	1 min
Tap water	3 min
Hematoxylin	3 min
Tap water	30 sec 3x
Dip (fast) in acid alcohol (200ml of 70% alcohol + 500 µl of HCl)	
DI water	15 min
Eosin	2 min
Tap water	2 min 2x
90% Ethanol	1 min
100% Ethanol	1 min

Xylene	2 min
Mounting media & coverslip	

Silver Staining. The distribution and localization of Ag-NPs and Au-NPs in the cell nucleus were validated with a silver staining Kit following manufacturer's protocol (Invitrogen Co., Thermo Fisher Scientific, Cat. LC6070). Briefly, after sample fixation, 30 % of ethanol was added to the samples for 10 minutes. The sensitizing solution was added, followed by 30 % ethanol, 10 minutes each. The samples were washed with ultrapure water and incubated in a staining solution for 15 minutes. The samples were washed again with ultrapure water for 20-60 seconds and incubated in the developing solution for 4-8 minutes. Lastly, stopper solution was added and gently agitated for 10 minutes, followed by washing with ultrapure water for 10 minutes. The resultant deposits of metallic silver around NPs were visualized using the spectral imaging system.

Statistics. Most of our statistical analysis was conducted by using Spectral Imaging software GenASI™ SpectraView version 7.2.7.34276 and GraphPad Prism software version 8.4.2. Microsoft Excel software version 16.37 was also used for linear regression analyses to obtain a standard calibration curve and linear equation. We used Student t-test to compare 2 groups and ANOVA followed by Tukey's posthoc test to compare 3 or more groups. A minimum of 3 independent studies was performed, and a more accurate repeat (*N*) was indicated in each figure by the dot plots and/or figure legend. Whenever possible, our studies were conducted in pairs by including control groups in each experimental group. The correlation analyses were performed by using Pearson correlation coefficient test. All data were reported as mean ± standard error of mean (SEM). While $P<0.05$ was considered significant, the level of significance was indicated accurately in each graph and figure legend.

Reference

1. R. Pala, A. M. Mohieldin, K. Shamloo, R. T. Sherpa, S. H. Kathem, J. Zhou, Z. Luan, J. G. Zheng, A. Ahsan and S. M. Nauli, *Nano Lett*, 2019, **19**, 904-914.
2. R. Pala, A. M. Mohieldin, R. T. Sherpa, S. H. Kathem, K. Shamloo, Z. Luan, J. Zhou, J. G. Zheng, A. Ahsan and S. M. Nauli, *ACS Nano*, 2019, **13**, 3555-3572.
3. Q. A. Alshammari, R. Pala, N. Katzir and S. M. Nauli, *Sci Rep*, 2021, **11**, 2703.